1-1-2015

Species Preference of Viral Deubiquitinating Proteases Toward ISG15 Through Structural and Enzymatic Characterization

Michelle Kay Deaton
University of Denver

SPECIES PREFERENCE OF VIRAL DEUBIQUITINATING PROTEASES TOWARD ISG15 THROUGH STRUCTURAL AND ENZYMATIC CHARACTERIZATION

_____

A Dissertation

Presented to

the Faculty of Natural Sciences and Mathematics

University of Denver

_____

In Partial Fulfillment

of the Requirements for the Degree

Doctor of Philosophy

_____

by

Michelle K. Deaton

June 2015

Advisors: Scott D. Pegan, Ph.D.

and Martin Margittai, Ph.D.

Author: Michelle K. Deaton
Title: SPECIES PREFERENCE OF VIRAL DEUBIQUITINATING PROTEASES TOWARD ISG15 THROUGH STRUCTURAL AND ENZYMATIC CHARACTERIZATION
Advisors: Scott D. Pegan, Ph.D. and Martin Margittai, Ph.D.
Degree Date: June 2015

ABSTRACT

Proteases from the Ovarian Tumor domain (OTU) superfamily of deubiquitinating enzymes (DUBs) are expressed by a range of RNA viruses. Viral OTUs (vOTUs) are found in nairoviruses such as Crimean Congo Hemorrhagic Fever virus (CCHFV), Nairobi sheep disease virus (NSDV), the Erve virus (ERVEV), and the Dugbe virus (DUGV), as well as in the areterivirus Porcine Reproductive and Respiratory Syndrome virus (PRRSV), among others. vOTUs, which interfere with host innate immune response through editing of host Ub and Ub-like molecules such as interferon stimulated gene 15 (ISG15), have been identified as a potential virulence factor through their role in evading the innate immune response. Study and characterization of vOTUs involves evaluating their activity and preferences for Ub, ISG15, as well as the variety of poly-Ub linkages that can form. While previous studies have compared vOTUs among different viruses, it was not known how vOTUs from differing strains of the same virus vary. To investigate vOTUs from differing strains of the same virus, vOTUs from two strains of PRRSV were selected. The vOTU of a highly pathogenic PRRSV strain, JXwn06, and a strain used in vaccination, MLV, were enzymatically characterized. Intriguingly, the JXwn06 vOTU displayed a strong preference for K63 linked di-Ub, with over 40-fold greater activity than the MLV vOTU. Additionally, neither strain showed significant activity towards ISG15, which is intriguing, as, at one point, it was believed

that deISGylating activity was a property of all vOTUs. In contrast to these PRRS vOTUs, a strong deISGylating enzyme, the ERVE vOTU, was selected for enzymatic and structural investigation. ERVE vOTU was found to not only prefer ISG15 over Ub, but recognized both mouse and human ISG15. In order to gain insight into this ability to recognize more than one species of ISG15, the X-ray crystal structure of the ERVE vOTU in complex with the C-terminal domain of mouse ISG15 (CmISG15) was elucidated to 2.47 Å. This structure not only revealed the structural configuration of the ERVE vOTU in complex with its substrate, but also provides the first structural information for mISG15. Key areas of binding were identified upon comparison of the manner in which ERVE vOTU recognizes the mouse analog of ISG15 with CCHF vOTU substrate binding. These key regions were explored through site-directed mutagenesis to determine if mutation at key binding areas would allow CCHF vOTU to more tightly bind mISG15. Based on CCHF vOTUs apparent lack of recognition of mISG15, special ISG15 constructs were designed to allow for testing against a panel of ISG15s from varying species.

In another area of interest, adenylosuccinate lyase (ADSL) was structurally and enzymatically investigated to build understanding of ADSL deficiency, a rare autosomal recessive disorder, which causes a defect in purine metabolism resulting in neurological and physiological symptoms. To better understand the causation of disease due to the R303C mutation, the wild type (WT) and the R303C mutant of ADSL were investigated enzymatically and thermodynamically. Additionally, the X-ray structures of ADSL in its apo form as well as with the R303C mutation were elucidated, providing insight into ADSL's cooperativity.

TABLE OF CONTENTS

LIST OF FIGURES

LIST OF TABLES

CHAPTER ONE: THE VOTU DOMAIN OF HIGHLY-PATHOGENIC PORCINE REPRODUCTIVE AND RESPIRATORY SYNDROME VIRUS DISPLAYS A DIFFERENTIAL SUBSTRATE PREFERENCE

Introduction

Porcine reproductive and respiratory syndrome virus (PRRSV) is a rapidly evolving virus which emerged as a serious pathogen of swine in the late 1980's, and has since become one of the most significant concerns to the global pork industry. These concerns have only been exacerbated by the emergence in 2006/2007 of highly pathogenic PRRSV (HP-PRRSV) in China and Southeast Asia (Li et al. 2007, Wu et al. 2009, Guo, Lager, Henningson, et al. 2013). More contemporary PRRSV isolates have been observed in Southeast Asia that show significant continuing evolution from the original 2006 isolates, but still retain the highly pathogenic phenotype (Yu et al. 2012, Guo, Lager, Schlink, et al. 2013). These observations underscore the need to mechanistically understand what is responsible for the increased virulence of HP-PRRSV, which is further complicated by the complex and poorly understood virulence determinants of the broad and genetically diverse PRRSV strains.

Upon infection with PRRSV, viremia is typically established in 6-12 hours and virus shedding has been observed for up to 157 days (Wills et al. 1997). It is likely that the prolonged time to virus clearance is directly related to the immunosuppressive effects of PRRSV infection. Although the mechanisms through which PRRSV subverts the

adaptive immune response have been mostly determined (Sang, Rowland, and Blecha 2011, Yoo et al. 2010, Charerntantanakul, Platt, and Roth 2006), the manner in which some strains of PRRSV initiate a comprehensive campaign against the innate immune response have not. Specifically, mechanism behind the apparent dysregulation of several innate immune pathways such as the type I interferon/IRF/NF-κB mediated innate immune pathways in cultured cells (Sun et al. 2010, Sun, Han, et al. 2012, Fang et al. 2012, Beura et al. 2010, Song, Krell, and Yoo 2010, van Kasteren et al. 2013), have remained elusive.

PRRSV is a positive-sense, single-stranded RNA virus in the genus *Arterivirus* of the family *Arteriviridae*. Phylogenetic analysis of PRRSV reveals two genetically distinct genotypes: Type 1/European PRRSV (type strain Lelystad) and Type 2/North American PRRSV (type strain VR-2332), with the HP-PRRSV isolates belonging to a distinct subgroup of Type 2. It is important to note, however, that due to a high rate of mutation and recombination, it is likely that actual genetic diversity of PRRSV continuously surges ahead of our ability to discover and characterize it (Shi et al. 2010). The PRRSV genome is 15 to 15.5 kb, and contains at least 10 open reading frames (ORFs), with 12 non-structural proteins (nsp) (Chand, Trible, and Rowland 2012). Due to the high degree of variability in nsp2, it remains likely that functional differences exist in nsp2 between various PRRSV isolates that might have consequences on strain virulence.

PRRSV nsp2 is a large, highly variable protein encoded in the ORF1a region of the genome as part of a larger polyprotein precursor (Snijder et al. 1995, Han, Wang, and Faaberg 2006, van Hemert and Snijder 2008). Nsp2 is liberated from this precursor via cleavage of the nsp1β:nsp2 junction by the nsp1β protease and cleavage of the nsp2:nsp3

junction by the intrinsic protease activity of nsp2 (den Boon et al. 1995, Snijder et al. 1995, van Hemert and Snijder 2008, Han, Rutherford, and Faaberg 2009). This protease activity resides within an amino-terminal region of nsp2 containing a papain-like cysteine protease domain (PLP2) that cleaves at a conserved GG dipeptide between nsp2 and nsp3 (Han et al. 2009, Ziebuhr, Snijder, and Gorbalenya 2000, Mielech et al.). It has also been shown bioinformatically that this PLP2 domain is part of a larger family of mammalian proteins known as the ovarian tumor domain (OTU) proteases (Frias-Staheli et al. 2007). This subgroup of viral OTU domains (vOTU) have been biochemically shown to act as deubiquitinases (DUB) of varying specificities and activities, capable of interfering with innate immune responses via dysregulation of ubiquitin (Ub) or ISG15 related protein signaling (Frias-Staheli et al. 2007, Capodagli et al. 2011, Akutsu et al. 2011, Capodagli et al. 2013).

Ub is involved in a number of cell signaling pathways through attachment to host protiens in a variety of linkages of poly-Ub chains. These poly-Ub chains form via an isopetide bond between the C-terminus of one Ub with either the N-terminus, or one of seven other lysine residues, of another Ub molecule. Both mono- and polyubiquitination of host proteins act as key regulatory steps in multiple distinct cell signaling pathways (Komander, Clague, and Urbe 2009, Kulathu and Komander 2012). One relevant example of this is the use of K63-linked poly-Ub in the activation of retinoic acid-inducible gene I/mitochondrial antiviral signaling protein (RIG-I/MAVS) (Zeng et al. 2010), linear poly-Ub-dependent activation of inhibitors (IκB kinases) of nuclear factor kappa-light-chain-enhancer of activated B cells (NF-κB) (Tokunaga et al. 2009), and K48-linked poly-Ub to trigger degradation of IκB and activation of NF-κB signaling

(Chen et al. 1995, Alkalay et al. 1995). Alternative forms of ubiquitination (K6, K11, K27, K33) have been implicated in other cellular functions, including lysosome/vesicle trafficking, DNA damage response, inhibition of protein degradation, mitochondrial damage/autophagy, endoplasmic reticulum (ER) associated protein degradation, T-cell activation, and tumor necrosis factor-alpha (TNFα) signaling (Kulathu and Komander 2012). Further, there exist multiple Ub-like proteins, such as interferon (IFN) stimulated gene 15 (ISG15), for which there are diverse functions and regulatory pathways including anti-viral host defense (Zhao et al. 2013). It is clear from this diverse and interwoven set of processes that it is insufficient to simply define a protease as a vOTU or DUB and subsequently ascertain the global picture of downstream cellular effects.

Herein, we describe detailed biochemical characterization of the vOTU activity of the PLP2 domain from a HP-PRRSV strain (JXwn06), and contrast that activity to that from the PLP2 domain of the avirulent modified live virus vaccine strain Ingelvac PRRS® (MLV). To do this, we utilized purified vOTU domains in an *in vitro* activity assay with chemically defined, purified substrates. This system provides significant advantages to *in cellulo* and *in vivo* activity assays, including the ability to directly query substrate preference and observe simplified reaction kinetics. Further, these assays avoid complications due to off-target effects or effects on complex cellular pathways which can make data interpretation problematic. Using this approach, we demonstrate that both the MLV and JXwn06 vOTU/PLP2 domains showed DUB activity on K48-Ub and K63-Ub substrates. Interestingly, the PLP2 domain from HP-PRRSV strain JXwn06 displayed significantly greater activity against K63-Ub substrates than the PLP2 domain of MLV. This represents the first report of a biochemical activity unique to HP-PRRSV that has

potential implications for increased immunosuppression and may contribute to the increased virulence exhibited by this Asian HP-PRRSV strain.

Experimental Procedures

Construction of OTU Domains and Porcine proISG15

Ingelvac PRRS® nsp2 nucleotides 1342-1986, coding for nsp2 aa 1-215, were inserted downstream of a 6x histidine tag, codon optimized for expression in E. coli, and used to synthesize the viral OTU polypeptide (MLV vOTU) (GenScript, Piscataway, NJ). A JXwn06 vOTU polypeptide representing nsp2 aa 1-215 was produced in a like manner. The coding sequence for porcine proISG15 (NM_0011286469) was codon optimized for expression in *E. coli*, and internal restriction endonuclease recognition sequences were altered by silent mutagenesis for cloning purposes (Huang et al. 2009). This optimized gene was synthesized with an amino terminal 3X FLAG-Tag and 10X His-Tag, as well as NcoI and BamHI sites for cloning purposes at the 5' and 3' ends, respectively (GenScript). This synthetic gene was subcloned into pET26b (EMD Millipore) for bacterial expression and purification.

Protein Purification

Porcine proISG15 (pproISG15) was purified from *E. coli* BL21(DE3) cells harboring the gene for pproISG15 grown at 37 ˚C in 6 L of LB broth containing 100 µg/mL of ampicillin until the optical density at 600 nm reached 0.6. Expression of pproISG15 was induced by the addition of IPTG to a final concentration of 0.5 mM at 20 ˚C overnight. The cells were resuspended in cold Buffer A (50 mM Tris [pH 7.5], 1 mM EDTA, and 20% (w/v) sucrose), and then centrifuged at 6700 x g for 30 minutes. The cells were then resuspended in 5 mM $MgCl_2$. The suspension was centrifuged at 6700 x g

for 30 minutes, and the protein was purified from the supernatant via Ni-NTA affinity, followed by size-exclusion chromatography on a Superdex75 using Buffer B (200 mM NaCl, 20 mM HEPES [pH 7.5], 2 mM DTT). The protein was further purified by cation exchange using a 10/100 MonoS column. The protein was eluted using a gradient from Buffer C (100 mM NaCl, 50 mM ammonium acetate [pH 4.5]) to Buffer D (1000 mM NaCl, 50 mM ammonium acetate [pH 4.5]). The vOTU from Crimean Congo hemorrhagic fever (CCHFV vOTU) was purified as described previously (Capodagli et al. 2011).

Fluorescent vOTU Deubiquitination and DeISGylation Assays

All assays were performed in duplicate in Buffer E (100 mM NaCl, 50 mM HEPES [pH 7.5], 0.01 mg/mL bovine serum albumin (BSA), 5 mM DTT) using a Corning Costar half-volume black 96-well plate with a reaction volume of 50 μL. The rates of the reactions were observed using an Infinite M1000 series plate reader (Tecan, Inc.). Specifically, the increase in fluorescence (excitation λ, 360 nm; emission, 460 nm) of 7-amino-4-methylcourmarin (AMC) upon cleavage from hUb-AMC, hISG15-AMC, (Boston Biochem, MA) and ZRLRGG-AMC (Bachem) substrates was monitored for JXwn06 and MLV vOTU (GenScript). To calculate turnover rates for 1 μM hISG15-AMC, 1 μM hUb-AMC, and 50 μM ZRLRGG-AMC, 1 μM, 4 nM, and 4 μM of enzyme were used against hISG15-AMC, hUb-AMC, and ZRLRGG-AMC, respectively.

The turnover rates for poly-Ub fluorescence resonance energy transfer (FRET) linkage substrates K11, K48, and K63 (Boston Biochem, MA) were determined by monitoring the increase in fluorescence (excitation λ, 544 nm; emission, 572 nm) resulting by the separation of a FRET TAMRA/QXL pair. Cleavage of three

commercially available FRET TAMRA/QXL pair configurations per K48 and K63 poly-Ub linkage FRET substrates were assessed. Each di-Ub FRET substrate at 1 μM was evaluated against an enzyme concentration of 500 nM.

Gel Shift Assays

Poly-Ub linked by the different isopeptide bonds (K6, K11, K29, K33, K48, and K63), as well as the N-terminal peptide bond (linear), were purchased from Boston Biochem, MA. K27 linked di-Ub was purchased from Ubiquigent. Dimeric-Ub substrates (10 μM) were incubated with 500 nM JXwn06 or MLV vOTU in reaction Buffer F (100 mM NaCl, 50 mM HEPES [pH 7.5], and 2 mM DTT) at 37 ˚C. Reactions were stopped at various times over 1 hour by mixing 9 μL of each reaction with 2 × SDS-Tricine sample buffer and heating at 95 ºC for 5 minutes. Results were visualized on 10 – 20% Mini-PROTEAN® Tris-Tricine Precast Gels (Bio-Rad, CA). For vOTU cleavage of trimeric K48 and K63 linkages, 20 μM of tri-Ub substrates were tested and analyzed in the same manner as di-Ub.

10 μM hproISG15, (Boston Biochem, MA) was incubated at 37 ˚C with 20 nM CCHFV vOTU, 14 μM MLV, or 20 μM JXwn06 vOTU. 10 μM pproISG15 was incubated at 37 ˚C with 20 nM CCHFV vOTUs. ProISG15 gel shift assays were tested and analyzed in the same manner as di-Ub. The concentrations of MLV and JXwn06 used were the maximum allowable concentration possible for this assay.

Assay for vOTU Cleavage of Porcine proISG15 by Anti-FLAG® Western Blotting.

The pproISG15 cleavage assays were assembled as described above in reaction buffer F, containing 10 μM pproISG15, and either 100 nM CCHFV vOTU or 1000 nM PRRSV vOTU domain. Reactions were incubated at 37 ºC, and aliquots were removed at

time 0, 1, 2, 5, 10, 30, and 60 minutes, as well as at 24 hours. Reaction progress was halted by addition of the removed aliquots to an equal volume of SDS-PAGE loading buffer and storage at -20 ºC until electrophoresis.

Timepoint samples for pproISG15 cleavage assays were separated by 10% Tris-Tricine SDS-PAGE, and resolved proteins were transferred to a PVDF membrane using the iBlot transfer apparatus (Life Technologies). The membrane was blocked with 3% milk in PBS and immunoblotted with a 1:3000 dilution of mouse α-FLAG® monoclonal antibody (Sigma-Aldrich; F1804). Proteins were detected using a 1:15000 dilution of peroxidase conjugated goat α-mouse IgG antibody (Zymax, Life Technologies) and the ECL Plus substrate (Pierce). Immunoblots were visualized using blue light fluorescence in a G:BOX imager (Syngene).

Results

Sequence Comparison of PRRSV strain JXwn06 and MLV vOTU domains

The vOTU domains of very few strains of PRRSV have been directly examined for suppression of innate immunity in cell culture. Two such studies utilized SD01-08 (a Type 1 isolate) (Sun et al. 2010) or VR-2332 (van Kasteren et al. 2012), which both cause only mild disease *in vivo*, and neither of which included an assessment of enzyme kinetics. Another study examined the ability of HP-PRRSV strain 07HBEZ vOTU to suppress IFN-β induction *in vitro* (Li et al. 2010). To more precisely examine and compare vOTU domain enzymatic activity and specificity for PRRSV strains of differing pathogenicity, the vaccine derivative, Ingelvac PRRS® MLV and HP-PRRSV strain JXwn06 were chosen for analysis. A vOTU domain alignment of these two PRRSV strains compared to a related arterivirus (equine arteritis virus; EAV) and CCHFV was

produced, using the catalytic and zinc-binding residues as alignment signature amino acids (Fig. 1). The two PRRSV strains display 83.7% identity/84.2% similarity within the designated vOTU region, while this domain displays ~21% identity between both PRRSV strains and EAV, and only ~10% identity between PRRSV and CCHFV.

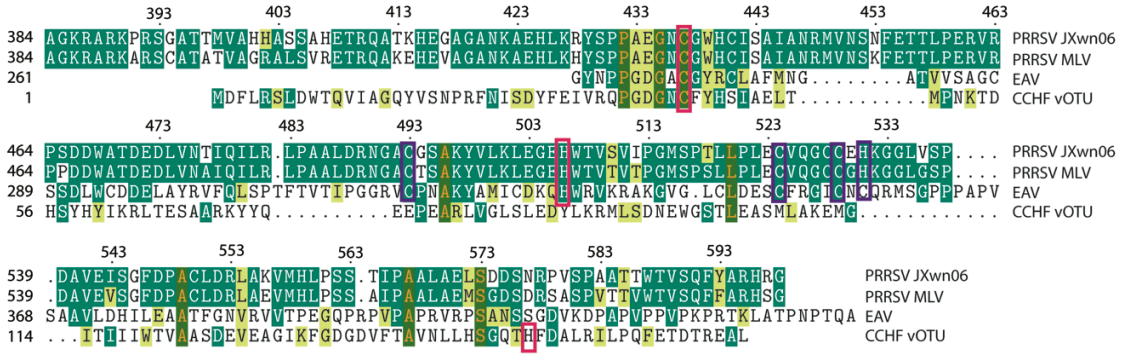

Figure 1: Sequence alignment of vOTUs. Sequence similarity is indicated as non-conserved (white background, black text), similar (yellow background, black text), conserved (green background, white text), or all matching (dark green background, orange text). Catalytic residues are boxed in red, and zinc-binding residues are boxed in purple. PRRSV sequence numbering is based on the residue number within nsp2.

Characterization of Strain Specificity

In order to investigate potential functional differences between vOTU domains from different PRRSV strains, we obtained biochemical data on the activity and specificity of PRRSV vOTU domains from strains JXwn06 and MLV. Initially, enzymatic activity was assessed utilizing Ub and ISG15 substrates, as well as a peptide substrate comprised of the five C-terminal amino acids common to Ub and ISG15, RLRGG (Fig. 2). By monitoring the release of the aminomethylcoumarin fluorophore from the C-terminus of these substrates, rate and substrate preference data was obtained. The vOTU domains originating from JXwn06 and MLV possess a noteworthy ability to cleave human Ub-AMC (hUb-AMC) conjugates, at 3.67 ± 0.04 and 2.30 ± 0.04 min^{-1}, respectively. However, when these vOTUs were assessed for activity against human

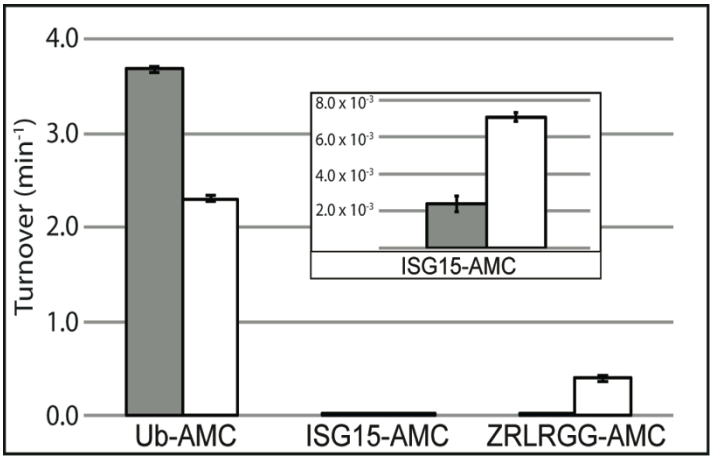

Figure 2: Kinetic data for fluorescence based assay. JXwn06 vOTU data is shown in gray and MLV vOTU data is shown in white. ISG15-AMC data is shown in the insert for clarity. Turnover number of substrate is measured as increase in fluorescence as AMC is cleaved off of the substrate molecule.

ISG15-AMC (hISG15-AMC), the vOTUs of JXwn06 and MLV exhibited activity 2,500 and 320 times less than their activities toward Ub-AMC, respectively. Interestingly, when assessed using the peptide substrate ZRLRGG-AMC, which is comprised of the last five conserved amino acids between Ub and ISG15, a large deviation in activity was observed between the vOTUs from MLV and JXwn06. Specifically, the activity of the MLV vOTU was 0.40 ± 0.04 min^{-1}, whereas JXwn06 vOTU was only $2.05 \pm 0.01 \times 10^{-2}$ min^{-1}. This result, as well as the dramatic difference between cleavage of Ub-AMC and hISG15-AMC, suggests a more complex interaction with the protein substrate beyond simple recognition of peptide sequence.

Di-Ubiquitin Specificity Divergence

In some cases, vOTU domains have been shown to have higher turnover rates for poly-Ub than for Ub-AMC due to an increase in the number of favorable contacts to which the enzyme can bind the substrate (Capodagli et al. 2013). Although the activity for mono-Ub was found to be relatively similar between JXwn06 and MLV vOTUs,

differences in rates of cleavage for di-Ub may exist between strains. To more precisely differentiate the di-Ub specificities of the JXwn06 and MLV vOTU domains, a panel of varying di-Ub substrates (composed of K6, 11, 27, 29, 33, 48, 63 and linear di-Ub linkages; Fig. 3a) was screened for activity. Both vOTU domains had an overall trend of

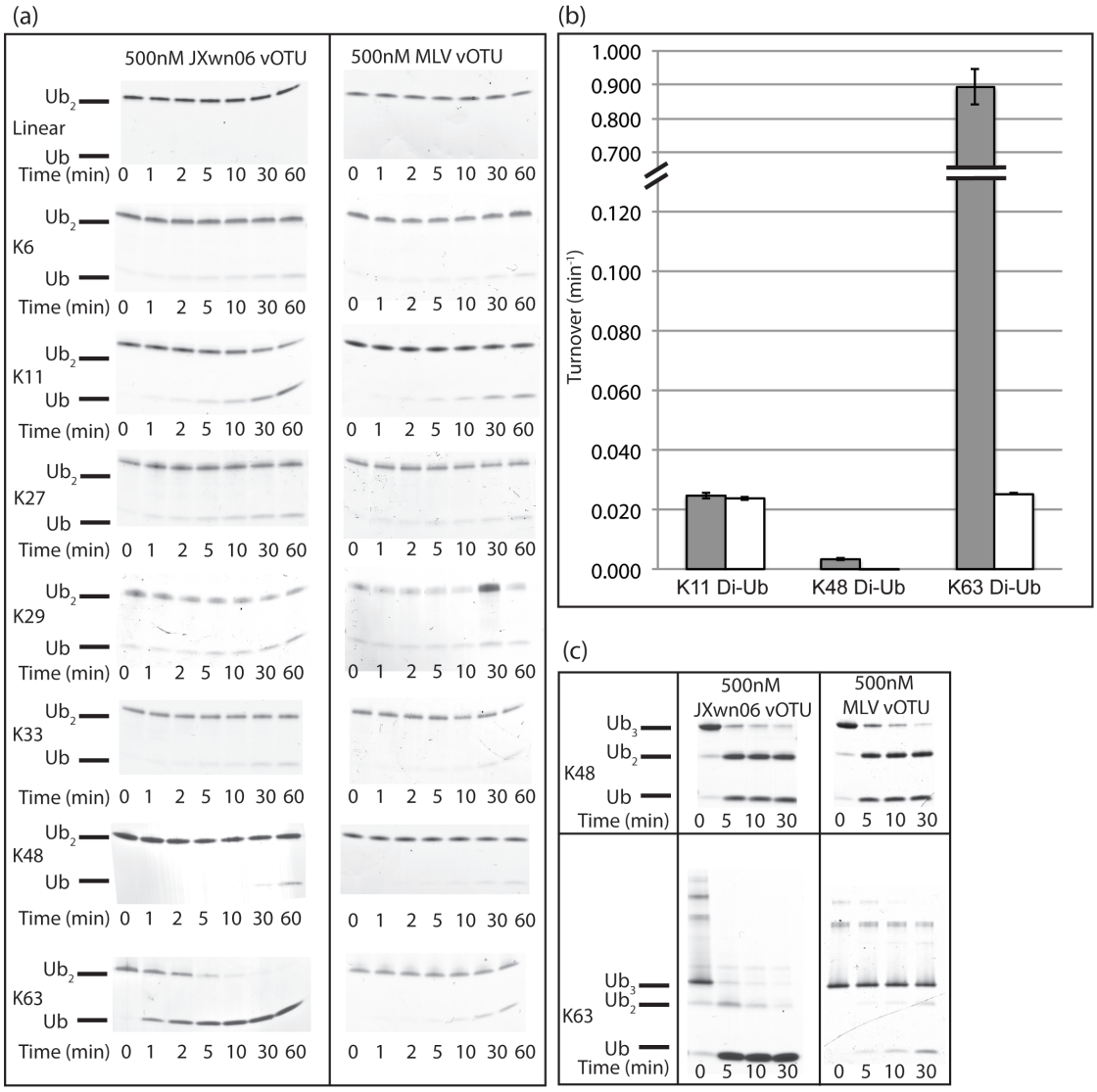

Figure 3: Cleavage of di- and tri- Ub. (a) Cleavage of various di-Ub linkages by JXwn06 and MLV vOTUs. (b) Kinetic data for FRET based Di-Ub assay. JXwn06 vOTU data is shown in gray and MLV vOTU data is shown in white. (c) Cleavage of tri-Ub by JXwn06 vOTU and MLV vOTU.

highest activity towards K63 linked di-Ub, followed, in descending order, by K11, K29, K6, K27, and K48-linkage, with no detectable activity toward linear linked di-Ub. Interestingly, while the observed activity was similar for most di-Ub linkages, JXwn06 vOTU was markedly more active toward K63 di-Ub, cleaving nearly all of the substrate within 10 min, compared to the MLV vOTU, for which a significant proportion of uncleaved K63 substrate remained after 60 min. In order to quantify the difference in activity towards di-Ub substrates, cleavage of K11, K48, and K63 di-Ub FRET substrates was assessed. These results aligned with the di-Ub gel shift assays, with both vOTU domains displaying low activity towards K48 linked di-Ub, and disparate activities utilizing K63 linked di-Ub. The activity of the JXwn06 vOTU towards K63 linked di-Ub was determined to be approximately 40-fold higher than that of MLV vOTU (Fig. 3b).

To assess potential differences in vOTU domain activity on substrates similar to poly-Ub, activity assays were performed using K48 and K63 linked tri-Ub (Fig. 3c). In stark contrast to the K48 linked di-Ub substrate, both vOTU domains of MLV and JXwn06 rapidly cleaved the majority of K48 tri-Ub into di- and mono-Ub within 5 min. However, consistent with the previous results, the resulting K48 linked di-Ub appeared refractory to subsequent vOTU cleavage. As in the di-Ub cleavage assay, the K63 linked tri-Ub substrate was rapidly and completely cleaved to mono-Ub by the JXwn06 vOTU domain within 10 min. Unlike the surge in activity observed using K48 linked tri-Ub for the MLV vOTU domain, its cleavage of K63 linked tri-Ub proceeded at the same modest rate observed for K63 di-Ub.

Pro-ISG15 Activity

While Ub is highly conserved among species, ISG15 is more divergent, with human and porcine ISG15 sharing 67% sequence homology. Nairovirus vOTUs such as the CCHFV vOTU have previously been demonstrated to possess species specificity for ISG15 (Capodagli et al. 2013). To determine if the low hISG15-AMC activity observed for JXwn06 and MLV vOTU domains was also related to species specificity, cleavage of the pro-form of human (hproISG15) and porcine (pproISG15) were examined, using the CCHFV vOTU as a control. First, cleavage of hproISG15 was examined. At the low enzyme concentration of 20 nM, CCHFV vOTU cleaved the hproISG15 at a rate that was readily observed in the one-hour time trial (Fig. 4a). Since the PRRSV vOTUs exhibited much lower turnover numbers for hISG15-AMC, the highest allowable concentrations of MLV and JXwn06 were utilized. However, even at the increased concentrations for MLV and JXwn06 vOTUs, no cleavage of the hproISG15 was observed for either in the one-hour time span (Fig. 4a). When examining cleavage of pproISG15, while CCHFV vOTU was seen to cleave the pproISG15 at a significantly reduced rate to that of hproISG15, no cleavage of pproISG15 by JXwn06 and MLV vOTU domains was detected within a one-hour time course. It was only after an extended 24-hour incubation that a trace of cleaved product was observed (Fig. 4a, b).

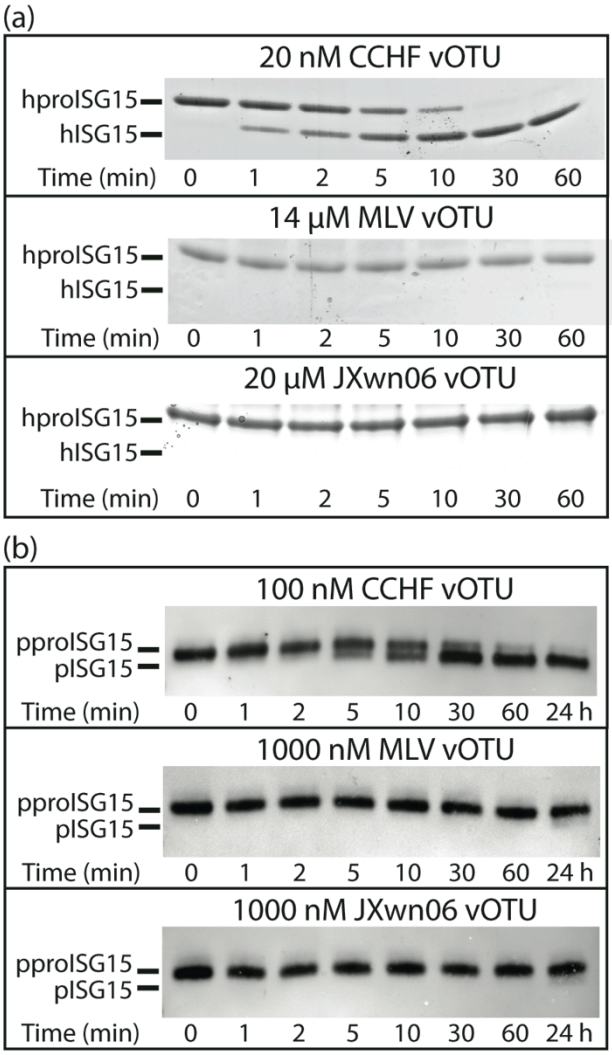

Figure 4: ProISG15 gel shift assay. (a) Cleavage of human (h) proISG15 by CCHFV, JXwn06, or MLV vOTU is shown over a one-hour time course and visualized by coomasie blue staining. (b) Cleavage of porcine (p) proISG15 by varying concentrations of CCHFV, JXwn06 and MLV vOTUs are shown over a one hour time course as well as a 24-hour time point. Cleavage products were visualized by anti-FLAG® western blot of tagged-pproISG15.

Discussion

The identification of a vOTU domain in nsp2 of the arterivirus PRRSV sets it among a number of viruses containing vOTUs, including nairoviruses, tymoviruses, a tenuivirus, and other nidoviruses. Recently, vOTUs from nairovirus representatives CCHFV, Dugbe virus and Erve virus (ERVEV), as well as the tymovirus prototypical member turnip yellow mosaic virus (TYMV) were probed extensively, and illustrated

vOTUs from different species can vary greatly in their preference for substrate (Capodagli et al. 2013). The vOTUs from JXwn06 and MLV follow this trend. Relative to previously characterized vOTU domains of viruses, JXwn06 and MLV vOTU domains displayed moderate deubiquitinating activity. The vOTUs previously probed have deubiquitinating activity which ranges from approximately 0.03 to 27 min^{-1} (Capodagli et al. 2013). The PRRSV vOTUs fall into the lower end of this range, with deubiquitinating activity closest in value to that of ERVEV vOTU, which is considered a poor deubiquitinating enzyme relative to other nairoviruses (Capodagli et al. 2013). However, relative to nairovirus counterparts, such as vOTUs from CCHFV and ERVEV, that clearly possess deISGylating activity, PRRSV vOTUs deISGylating activity is extremely low. Comparatively, other vOTUs have activity ranging from ERVEV vOTU at the high end, at 15 min^{-1}, to TYMV vOTU at the low end with activity of only 0.005 min^{-1}. The PRRSV vOTUs hISG15 activities are near the lower end of these reported vOTU activities, with similar values to the TYMV vOTU, whose plant host lacks an ISG15 homologue. Upon comparing the proteolytic activity of the PRRSV vOTUs toward the last five amino acids common to both Ub and ISG15 as measured by cleavage of ZRLRGG-AMC, a divergence in their comparative activities was found. The activity of the MLV vOTU is 20 times greater than that of the JXwn06 vOTU and 30% greater than the highest activity observed in the recent survey of representative vOTU domains reported by (Capodagli et al. 2013).

Further comparison and analysis of the vOTU domain from the highly pathogenic JXwn06 strain of PRRSV with the vOTU domain of the less pathogenic North American MLV strain revealed an intriguing result. The less virulent MLV vOTU maintained a

better proteolytic activity, as measured by fold change of relative cleavage of ZRLRGG-AMC, and the two vOTUs had similar moderate Ub-AMC activity. However, upon examining the activity of the two strain's vOTUs towards poly-linked Ub, rather than the mono-Ub-AMC, a large divergence in their activities was uncovered. The JXwn06 vOTU exhibited K63 linked Ub activity over 40 times greater than that of MLV, exemplifying how vOTUs with similar activity against mono-Ub may have divergent activity towards different di-Ub linkages. Suppression of K63 linked poly-Ub early in infection by JXwn06 may contribute to the increased disease severity in highly pathogenic PRRSV infection.

During initial examination of vOTU domains, such as that from CCHFV, it was theorized that all vOTUs might possess dual deubiquitinating and deISGylating activity. However, further work demonstrated that some vOTUs likely serve primarily as deubiquitinases, while others may have a stronger preference for ISGylated substrates (Capodagli et al. 2013). For PRRSV vOTU domains from Jxwn06 and MLV, both were found to not only have very low activity against hISG15-AMC, but were unable to appreciably cleave either pproISG15 or hproISG15. The latter experiment eliminates a species-specificity effect, as seen in CCHFV vOTU, as the primary driver for the absence of activity (Fig 4b,c). As a result, the lack of deISGylating activity suggests that PRRSV core domain may be more suited as a deubiqutinase than a deISGylase. The lack of deISGylating activity is surprising given that PRRSV nsp2 has been previously suggested to play a direct role in reducing the amount of ISGylation in cells (Sun et al. 2012). This may indicate additional protein requirements for cleavage of ISG15 by PRRSV vOTUs. These additional requirements may come in the form of accessory proteins, or in a

requirement for a larger domain within the nsp2 protein, as it has previously been demonstrated that larger proteolytically active domains of nsp2 were required for *trans* vs. *cis* cleavage specificities (Han, Rutherford, and Faaberg 2009). Alternatively, the observed cleavage of ISG15 modified proteins in cell culture may be due to an upstream effect of nsp2, rather than a direct effect of vOTU domain activity. Also, the extended time course inherent in cellular testing, coupled with the observed trace activity of PRRSV vOTUs for ISGylated substrates, may have permitted the gradual buildup of deISGylated substrates thereby exaggerating the magnitude of PRRSV vOTU's deISGylating activity. This is of particular importance, given the kinetics of the antiviral response, particularly in the early stages of viral infection.

PRRSV virulence and attenuation have been studied extensively, with most studies implicating multiple regions of the virus in contributing to virulence, consistent with the observation that individual PRRSV vaccines appear to have become attenuated by different mechanisms (Brockmeier et al. 2012, Wang et al. 2008, Kwon et al. 2008, Storgaard, Oleksiewicz, and Botner 1999, Ni et al. 2013, Nielsen et al. 2001, An et al. 2011, Shi et al. 2013, Ellingson et al. 2010, Yuan et al. 2001, Han et al. 2013, Kim et al. 2010, Song, Krell, and Yoo 2010). Narrowing the focus to the PLP2/vOTU region of nsp2, previous reports have generally demonstrated deubiquitinating activity of certain strains, leading to subsequent suppression of innate immune responses in infected cells (Frias-Staheli et al. 2007, van Kasteren et al. 2012, Sun et al. 2010, Li et al. 2010), suggesting a mechanistic role in PRRSV virulence. In this report, we have shown that the core vOTU domain (215 residues), which varies only 17% (amino acid identity) between different strains of PRRSV, was responsible for marked differences in K63-linked

deubiquitination, reinforcing the role of the PLP2/vOTU domain in virulence variation between PRRSV strains. It is important to note that this core domain must function primarily as a viral protease, placing significant constraints on evolution of secondary functions. This also underscores the complexities of PRRSV virulence, since MLV and its parental field isolate (VR-2332) share the identical vOTU domain sequence while exhibiting differential pathogenicity in swine. Therefore it is crucial to recognize that while differential vOTU activity may contribute to virulence, it remains one of a constellation of potential virulence factors. Mechanistically, several critical innate immune sensors and cellular anti-viral pathways utilize K63 ubiquitination as an essential activation step, such as RIG-I/MAVS, MDA5, and MITA/STING (Oshiumi et al. 2013, Jiang et al. 2012, Guo, Lager, Schlink, et al. 2013). Antagonism of these pathways by a vOTU domain with preference for K63-polyubiquitin could lead to a decrease in type I interferon production and NF-κB signaling, thereby abrogating or significantly delaying establishment of the anti-viral state. If K63 preference and increased deubiquitination activity of the JXwn06 vOTU domain is a shared characteristic of all highly-pathogenic PRRSV isolates, then it is possible that this unique activity contributes to the increased virulence of these strains.

CHAPTER TWO: IDENTIFYING FACTORS OF SPECIES PREFERENCE OF VOTUS FROM CCHFV AND ERVEV TOWARDS ISG15

Introduction

Nairoviruses are negative-sense single stranded RNA viruses, which infect both animals and humans. The genus includes 34 known viruses, of which the Crimean-Congo Hemorrhagic Virus (CCHFV), Dugbe Virus (DUGV), and Nairobi sheep virus (NSDV) have been the most investigated. The Erve nairovirus (ERVEV), which was isolated from the white-toothed shrew in 1982 in northwest Europe, has been implicated as a causative agent in human thunderclap headaches. Among nairoviruses, disease outcomes in humans can range from mild symptoms, such as headaches, as is the case with the Erve virus, to severe hemorrhaging, high fever and death with CCHFV (Capodagli et al. 2013).

Intriguingly, while CCHFV is often fatal in humans, it shows no signs of disease in a large range of infected animals. Likewise, NSDV, which is fatal in sheep, only causes mild febrile illness in humans. The most recently identified nairovirus, the Leopards Hill virus (LPHV), causes severe disease in mice (Ishii et al. 2014). It is currently unknown why severe disease is presented to only a single species infected with these nairoviruses. One key factor may lay in the ability of a nairovirus to efficiently circumvent the immune response of certain species. Recently, a potential nairovirus virulence factor, ovarian tumor domain protease (vOTU) found within the L-segment of

narioviruses' genome, was identified. Investigations into vOTU's preference for ubiquitin (Ub) and Ub-like proteins have revealed differing specificities toward different host's Ub-like interferon stimulated gene product 15 (ISG15). Specifically, the vOTU from CCHFV has been shown to be highly specific to human ISG15 (hISG15), while the vOTU from ERVEV can recognize both mouse and human ISG15. In order to further understand this behavior, a complex of the ERVE vOTU with the C-terminal domain of mouse ISG15 (CmISG15) was elucidated to 2.47 Å. Additionally, constructs of ISG15s of varying species in a designed pro-form were paneled against varying vOTUs to probe the vOTUs species preferences further.

Experimental Procedures

vOTU and CmISG15 Construct Design

For the ERVE vOTU expression construct, the first 171 amino acids from the L-protein in ERVEV (GenBank AFH89032.1), and for the NSD vOTU, the first 186 amino acids from the L-protein in NSDV (GenBank AED88229.1), which both correspond to the first 169 amino acids of CCHF vOTU (Fig. 5) and include the OTU domain as described by Dilcher et al. (2012) were utilized. Similarly to the CCHF vOTU construct, six histidines and a stop codon were added to ERVE vOTU and NSD vOTU constructs to generate a C-terminal histidine tag. ERVE vOTU was incorporated into pET11a plasmids using NdeI and BamHI restriction sites, and NSD vOTU was incorporated into pET28a. Addgene plasmid 12448 harboring mouse ISG15 (mISG15) in pET15b (mISG15-pET15b) as described in Kim and Zhang (2005) was obtained from Addgene. Cysteine 78 of mISG15 was mutated to a serine as described in Sorensen et al. (2007). The C-terminal

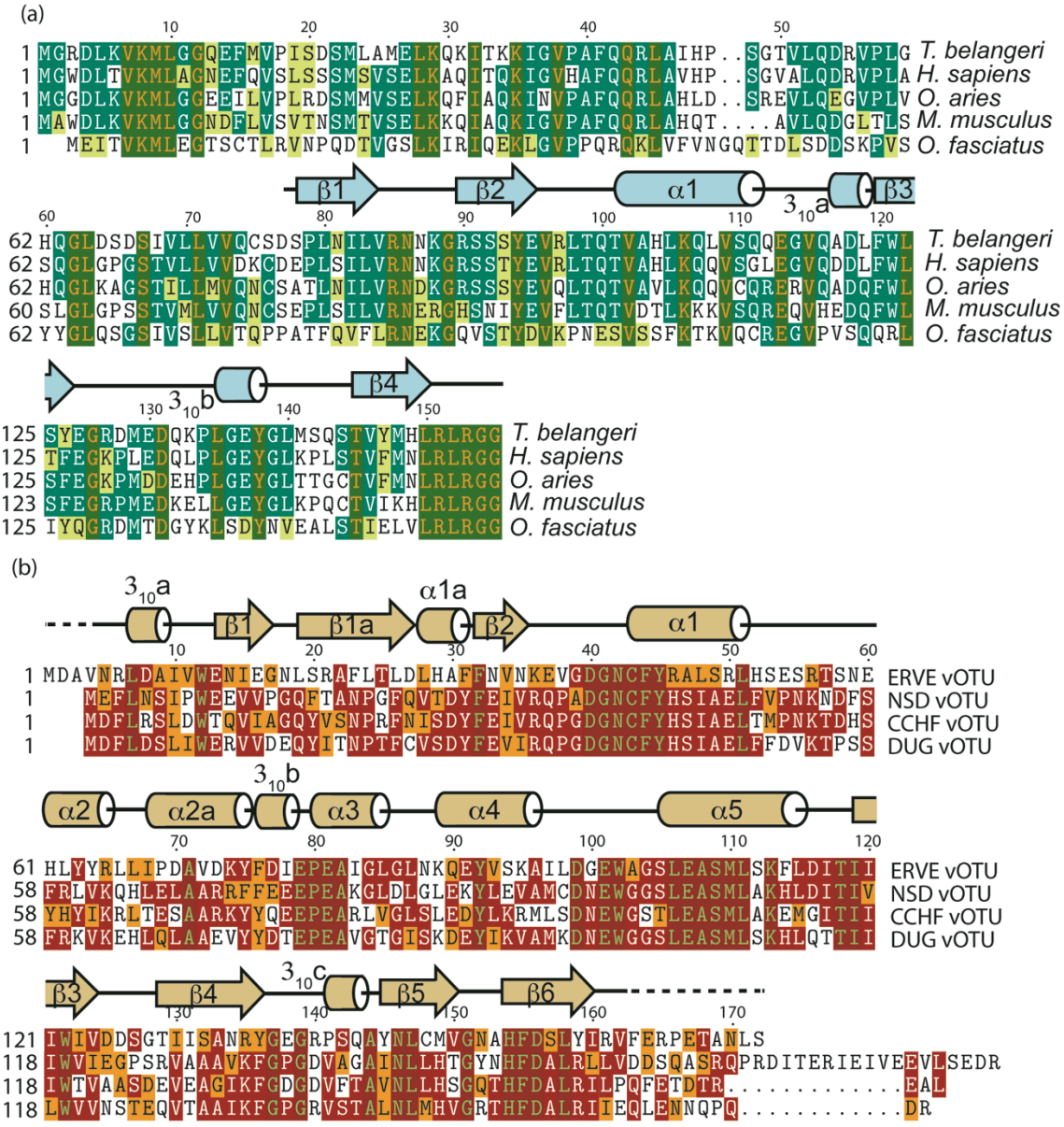

Figure 5: Sequence alignment of ISG15s and of vOTUs. (a) The ISG15 from *T. belangeri* (Northern tree shrew), *H. sapiens* (human), *O. aries* (sheep), *M. musculus* (mouse) and *O. faciatus* (jackknife fish) are shown aligned. The secondary structure of CmISG15 according to Defined Secondary Structure of Proteins (DSSP) is shown as blue cylinders (helices), blue arrows (beta sheets), and black lines (loops). (b) ERVE vOTU, NSD vOTU, CCHF vOTU, and DUG vOTU are shown aligned. The secondary structure of ERVE vOTU according to Defined Secondary Structure of Proteins (DSSP) is shown as tan cylinders (helices), tan arrows (beta sheets), and black lines (loops). Dashed lines represent regions for which electron density was not defined in the crystal structure.

domain of mISG15 (CmISG15) was amplified by PCR, and was then sub-cloned into pTYB2 using NdeI and SmaI restriction enzyme sites (CmISG15-pTYB2). A CmISG15

construct in pET15b (CmISG15-pET15b) was generated by PCR amplification of the entire mISG15-pET15b construct except the N-terminal domain, followed by NdeI digestion and then ligation. Additional constructs of ISG15 from the sheep *Ovis aries* (NCBI reference sequence NP_001009735.1), the northern tree shrew, *Tupaia belangeri* (GenBank AFH66859.1), and from the jackknife fish, *Oplegnathus faciatus* (GenBank BAJ16365.1) were designed with the same C-terminal additional amino acids as the pro form of human ISG15 (hproISG15) construct, GTEPGGRSGHHHHHH, generating constructs termed sheep-proISG15, Nshrew-proISG15, and fish-proISG15, respectively. These constructs were incorporated into pET15b using NdeI and BamHI restriction sites. The vOTU and ISG15 constructs were introduced into E. coli BL21 (DE3) competent cells by heat-shock transformation. The mISG15 construct was heat-shock transformed into BL21 (DE3)-CodonPlus competent cells. The resulting plasmids were then purified, restriction analyzed, and sequenced to verify the construct. The hproISG15 construct was purchased from Boston Biochem.

Expression of vOTUs and ISG15s

For vOTU enzymatic studies, *E. coli* harboring vOTUs from CCHFV, ERVEV, mISG15-pET15b, CmISG15-pET15b, or a proISG15 construct were grown at 37 ˚C in LB broth containing 100 μg/mL of ampicillin until the optical density at 600 nm reached 0.6. Expression of the vOTU, mISG15, CmISG15, or proISG15 gene was induced by the addition of IPTG to a final concentration of 0.8 mM. The culture was further grown for 4 hrs at 37 ˚C and then centrifuged at 6,000xg for 10 minutes. CmISG15-pTYB2 was grown similarly, but with an induction by the addition of IPTG to a final concentration of

0.5 mM, grown at 18˚C overnight. Mutants of vOTUs and CmISG15 were grown the same as their parent strains. Cells were collected and stored at -80 ˚C until use.

Purification of vOTUs and mISG15

All vOTUs were purified according to the previously published protocol (Capodagli et al. 2011). Purification of mISG15-pET15b was performed by enzymatically lysing cells resuspending cells in 500 mM NaCl, 50 mM Tris [pH 7.5], and 1 mM Tris (2-carbozyethyl) phosphine hydrochloride [TCEP-HCl] plus lysozyme. The solution was then sonicated on ice at 50% power on five seconds, off five seconds for 10 minutes total, using a Sonic Dismembrator Ultrasonic Processor (Fisher Scientific). Insoluble debris was removed by centrifugation at 17,000xg for 45 minutes. The clarified extract was filtered with a 0.80 μm filter and then poured over 2 mL of Ni-NTA beads. The beads were washed with 10 mL lysis buffer supplemented with 10 mM imidazole, and eluted with 10 mL lysis buffer supplemented with 250 mM imidazole. The elution was then injected on a Superdex75 size-exclusion column and eluted with a buffer containing 200mM NaCl and 50 mM HEPES [pH 8.0]. All final protein concentrations were determined by absorbance at 280 nm using calculated extinction coefficients (Gill and von Hippel 1989).

Purification of CmISG15-pTYB2 was performed by chemically lysing cells by resuspending cells in CmISG15 lysis buffer (25 mM HEPES pH 6.8, 50 mM sodium acetate, and 75 mM NaCl), augmented with 0.16% Triton X-100. The solution was then sonicated on ice at 50% power on five seconds, off five seconds for 10 minutes total. Insoluble debris was removed by centrifugation at 17,000xg for 45 minutes. The clarified

extract was filtered with a 0.80 μm filter and then poured over a chitin column pre-equilibrated with CmISG15 lysis buffer. The column was washed with three column volumes of CmISG15 lysis buffer, followed by resuspension of the beads in two column volumes of CmISG15 lysis buffer supplemented with 250 mM sodium 2-mercaptoethanesulfonate (MESNA). The resuspension was rocked gently overnight at 4 ˚C to allow the MESNA to cleave the CmISG15 protein off of its chitin binding fusion tag. The chitin bead / protein solution was poured into a XK 26/40 GE column and the flow-through was collected. The resulting CmISG15 thioester solution was then concentrated to reduce the volume to 20 mL. Then 480 μL 5 M NaOH and 1.84 g propargylamine were added to the CmISG15 thioester, which was then incubated overnight at 4°C to create the suicide substrate, CmISG15-PA. Purified ERVE vOTU was added directly to the solution containing CmISG15-PA in equi-molar ratios, and was incubated at room temperature for 4 hours to create the ERVE vOTU-CmISG15 complex. This protocol was adapted from previously described methods (Messick et al. 2008, Wilkinson, Gan-Erdene, and Kolli 2005), and is illustrated in Fig. 6. The complex was further purified by anion exchange chromatography, eluting from a GE MonoQ 10/100 column using a linear gradient from 50 mM Tris [pH = 7.3] to 50 mM Tris [pH = 7.3], 1 M NaCl, followed by size exclusion chromatography on an AP-1 (Waters) column packed with Superdex75 resin preequilibrated with 100 mM NaCl, 5 mM Hepes [pH = 7.5], 2 mM DTT.

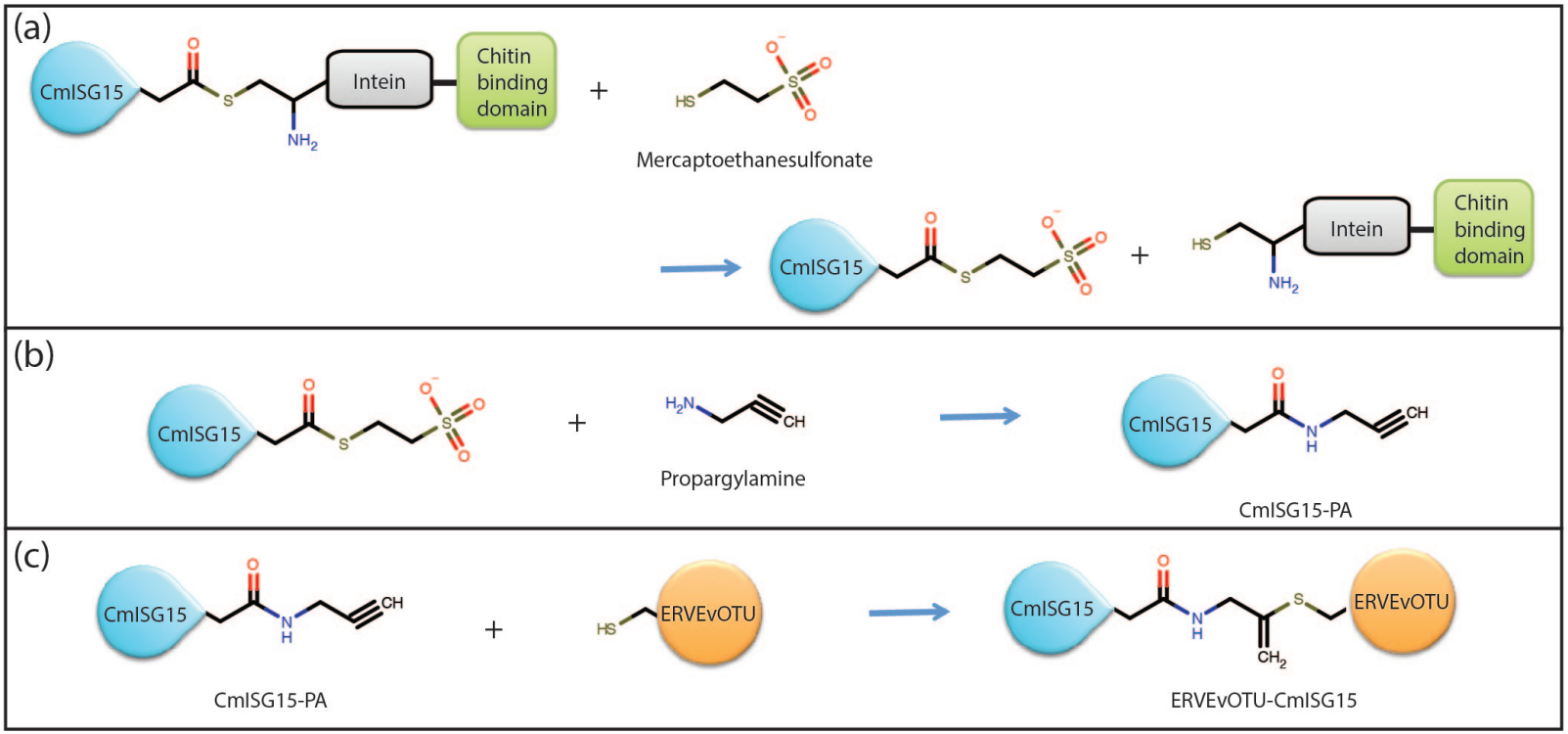

Figure 6: Generating ERVEvOTU-CmISG15 complex. (a) Cleavage of CmISG15 from Chitin binding domain fusion protein by mercaptoethanesulfonate. (b) Derivitization of C-terminus of CmISG15 by propargylamine (PA) to create suicide substrate CmISG15-PA. (c) Complexation of CmISG15-PA with ERVE vOTU to create covalently bound ERVEvOTU-CmISG15 complex for crystallization

Crystallization of ERVE vOTU-CmISG15

Purified ERVE vOTU-CmISG15 was concentrated to 12.5 mg/mL using Vivaspin 6 10-kDa MWCO concentrators and filtered using a 0.22 μm pore size Costar spin filter, and screened against a panel of QIAGEN NeXtal Suites using a TTP Labtech Mosquito. Initial screening resulted in several hits of needle-like crystals, the most viable of which formed in 6% PEG 6000, 0.1 M citric acid [pH = 4.6]. These were further optimized utilizing the Additive HT Screen from Hampton Research. Final rod-shaped ERVE vOTU-CmISG5 crystals were obtained through vapor diffusion using a 500 μL reservoir with 2 μL hanging drops mixed 1:1 with protein solution and reservoir solution supplemented with 0.2 μL 3.0 M NDSB-195. The crystal was transferred to a cryoprotective solution of 30% PEG 6000, 0.1 M citric acid [pH = 4.6], and then flash cooled in liquid nitrogen. The frozen crystal was mounted under a stream of dry N_2 at 100 K. An ERVE vOTU-CmISG15 data set with resolution of 2.47 Å was collected at the Advanced Photon Source (APS) beamline BM-22 at 1.00 Å with a MAR300hs detector. X-ray images were indexed, processed, integrated, and scaled using HKL2000 (Otwinowski and Minor 1997). An initial phase solution was elucidated using a homology model based on the DUB vOTU-Ub structure 4HXD using Phaser. The structure was refined using iterative cycles of model building and refinement using COOT and PHENIX, respectively (Emsley and Cowtan 2004, Adams et al. 2010). Water molecules were added to the 2Fo-Fc density peaks of $>1\sigma$ using the Find Water COOT program function. The final model was checked for structural quality using the CCP4

suite programs Procheck and Sfcheck. The data refinement statistics are shown in Table 1.

Table 1: Data Collection and Refinement Statistics

	Erve-CmISG15
Data Collection	
Space Group	$P4_3$
Unit Cell Dimensions	
a, b, c (Å)	66.0, 66.0, 122.0
α=β=γ (degrees)	90.0, 90.0, 90.0
Resolution (Å)	50.0-2.47
No. Reflections Observed	36,660
No. Unique Reflections	18,742
Rmerge (%)	13.6 (55.9)*
I/σI	11.5 (2.56)*
% Completeness	100.0 (100.0)*
Refinement	
Resolution Range	50.0-2.47
No. Reflections in Working Set	17,722
No. Reflections in Test Set	986
Rwork (%)	18.3
Rfree (%)	23.3
Mean B-factor ($Å^2$)	16.2
Protein B-factor ($Å^2$)	15.3
Water B-factor ($Å^2$)	22.5
RMS deviation:	
Bond Lengths (Å)	0.009
Bond Angles (degrees)	1.43
Protein / Water Atoms	3829/251
Monomers in Asymmetric Unit	2

* The last resolution shell is shown in parentheses.

a Rmerge=ΣhΣi|Ii(h)−⟨I(h)⟩|/ΣhΣiIi(h), where Ii(h) is the ith measurement and ⟨I(h)⟩ is the weighted mean of all measurements of I(h).

b Rwork and Rfree=h(|F(h)o|−|F(h)c|)/h|F(h)o| for reflections in the working and test sets.

Site Directed Mutagenesis

Mutants of CCHF vOTU were generated using QuikChange site-directed mutagenesis according to the manufacturer's protocol (Agilent Technologies, Inc.). The resulting mutant plasmids were introduced into *E. coli* XL1-Blue Supercompetent cells by heat shock transformation and were then propagated, purified for sequence verification, and transformed into *E. coli* BL21(DE3) cells for enzyme expression. The complete coding regions for all mutant enzymes were sequenced by Eton Bioscience, Inc.

Fluorescent deISGylation Assay

All assays were performed in duplicate in 100 mM NaCl, 50 mM HEPES [pH 7.5], 0.01 mg of bovine serum albumin [BSA]/ml, 5 mM dithiothreitol [DTT] using a Corning Costar half-volume black 96-well plate with a reaction volume of 50 µl. The rates of the reactions were observed using a CLARIOstar series plate reader (BMG LABTECH). Specifically, the increase in fluorescence (excitation λ, 360 nm; emission, 460 nm) of 7-amino-4-methylcourmarin (AMC) upon cleavage from human ISG15-AMC (hISG15-AMC) (Boston Biochem, MA) was monitored for each of the vOTUs. A calibration curve for AMC was generated by addition of excess vOTU to various concentrations of Ub-AMC, and the reactions were allowed to run until the fluorescence signal was no longer increasing with time. The resulting maximum fluorescence values were plotted to determine the slope and subsequently create a calibration curve.

Mouse ISG15 Competition Assay

The ability of 4 nM vOTU from CCHF vOTU and ERVE vOTU to cleave 2 µM hISG15-AMC in the presence of unlabeled mISG15 (120 µM) or hISG15 (120 µM) was

observed by measuring the increased fluorescence of free AMC (excitation λ, 360 nm; emission, 460 nm) on an Infinite M1000 series plate reader (Tecan). Unlabeled mISG15 was obtained as described above, whereas hISG15 was acquired from a commercial source (Boston Biochem). All assays were performed in buffer 200 mM NaCl, 50 mM HEPES [pH 8.0], 0.01 mg of BSA/ml, 5 mM DTT using a Corning Costar half-volume black 96-well plate with a reaction volume of 50 µl. The ability of 4 nM CCHF vOTU to cleave 1 µM hISG15-AMC in the presence of mISG15 (700 µM), or CmISG15 (700 µM) was measured as above using a CLARIOstar series plate reader (BMG LABTECH).

Pro-ISG15 Cleavage Assay

10 µM of purified sheep-proISG15, Nshrew-proISG15, or fish-proISG15, or hproISG15 (Boston Biochem, MA) were incubated with 20 nM CCHF, ERVE, NSD vOTU, or SARS PLpro in 100 mM NaCl, 5 mM HEPES [pH 7.5], and 2 mM DTT at 37 ˚C. Reactions were stopped at various times over 1 hour by mixing 9 µL of each reaction with 2 × SDS-Tricine sample buffer and heating at 95 ºC for 5 minutes. Results were visualized on 10 – 20% Mini-PROTEAN® Tris-Tricine Precast Gels (Bio-Rad, CA).

Results

Species Specificity of CCHF and ERVE vOTU for ISG15

Unlike Ub, which is highly conserved among eukaryotes, ISG15 and its known homologs contain significant sequence variability, even among mammals. Previously, studies have suggested that vOTUs may prefer to cleave hISG15 or equivalent homologs specific to the species they infect(Capodagli et al. 2011). To investigate the effect of species diversity in ISG15s on vOTUs' ability to cleave these conjugates, unlabeled

hISG15 and mISG15 were used as competitive inhibitors against vOTUs from CCHFV and ERVEV. Predictably, both vOTUs show >90% decreases in their abilities to cleave hISG15-AMC in the presence of unlabeled hISG15. However, the presence of unlabeled mISG15 has a divergent effect between the two vOTUs. For CCHF vOTU, mISG15 lacks appreciable ability to interfere with this vOTU's cleavage of hISG15-AMC, revealing that CCHF vOTU substantially prefers hISG15 to mISG15 (Fig. 7). Interestingly, ERVE vOTU is inhibited by approximately 30% at the same mISG15 concentration, suggesting that affinity for certain species' ISG15s, or homologs, may vary among nairovirus vOTUs.

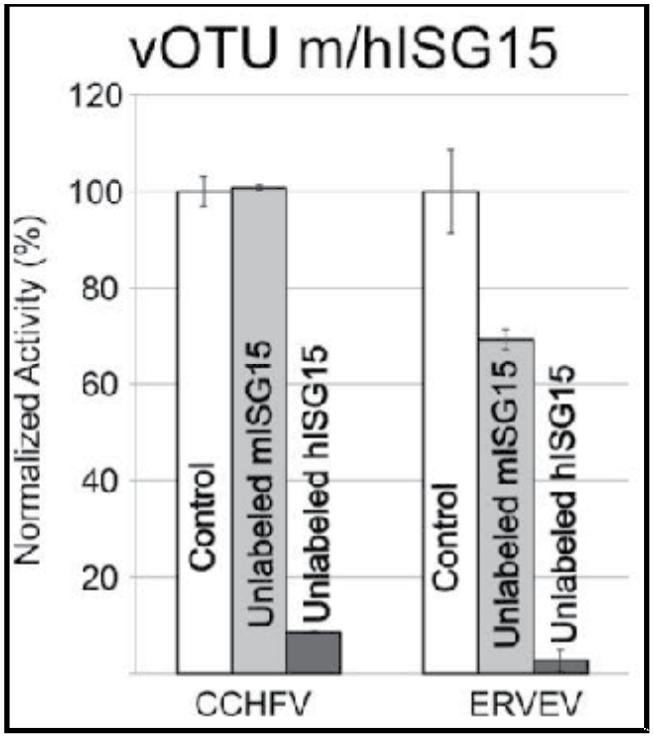

Figure 7: Inhibition of CCHF and ERVE vOTU by h/mISG15. Unlabeled m/hISG15 were evaluated as inhibitors of CCHF or ERVE vOTU in the hISG15-AMC assay.

X-ray Crystallographic Elucidation of ERVE vOTU-CmISG15 Structure

In order to further understand the structural basis for the multi-species recognition by ERVE vOTU, as well as elucidation of the structural features of CmISG15, a covalently bound complex of ERVE vOTU and CmISG15 (ERVEvOTU-CmISG15) was solved to 2.47 Å (Table 1). As has been found for other nairovirus vOTUs, CCHFvOTU and DUGvOTU, the ERVEvOTU possess similar global folds. It is composed of a core of seven β-sheets, flanked by seven α-helices, and three 3_{10} helices (Fig 8a). Interestingly, the ERVEvOTU-CmISG15 structure shared several similarities with the DUGvOTU-Ub (4HXD) structure reported by Capodagli et al. (2013). Specifically, it possesses the same shift at the alpha-3 helix seen with DUG vOTU when compared to CCHF vOTU. This helix is partly situated in a highly conserved amino acid sequence, which is flanked by more variable regions. In the middle of the α3-helix, where there is a transition from conserved to variable region, and positioned such that it is interfacing with the substrate binding interface, is CCHF vOTUs R80, which corresponds to Erve vOTUs I83. The corresponding ISG15 residues with which R80 and I83 interact are conserved between human and mouse ISG15. Interestingly, upon examination of vOTUs' interaction with their respective ISG15 substrate, the positively charged R80 and hydrophobic I83 each favorably interact with the conserved ISG15 region (Fig 8d-f). The hISG15 is situated such that its E132 is interacting with CCHF vOTUs R80, and P132 is shifted away. Similarly, the mISG15 is shifted such that its P128 is hydrophobically interfacing with ERVE vOTUs I83, while its E130 is not involved in binding (Fig 8d). This shift is driven by the variation in the vOTU, not the substrate. Variations in substrates are

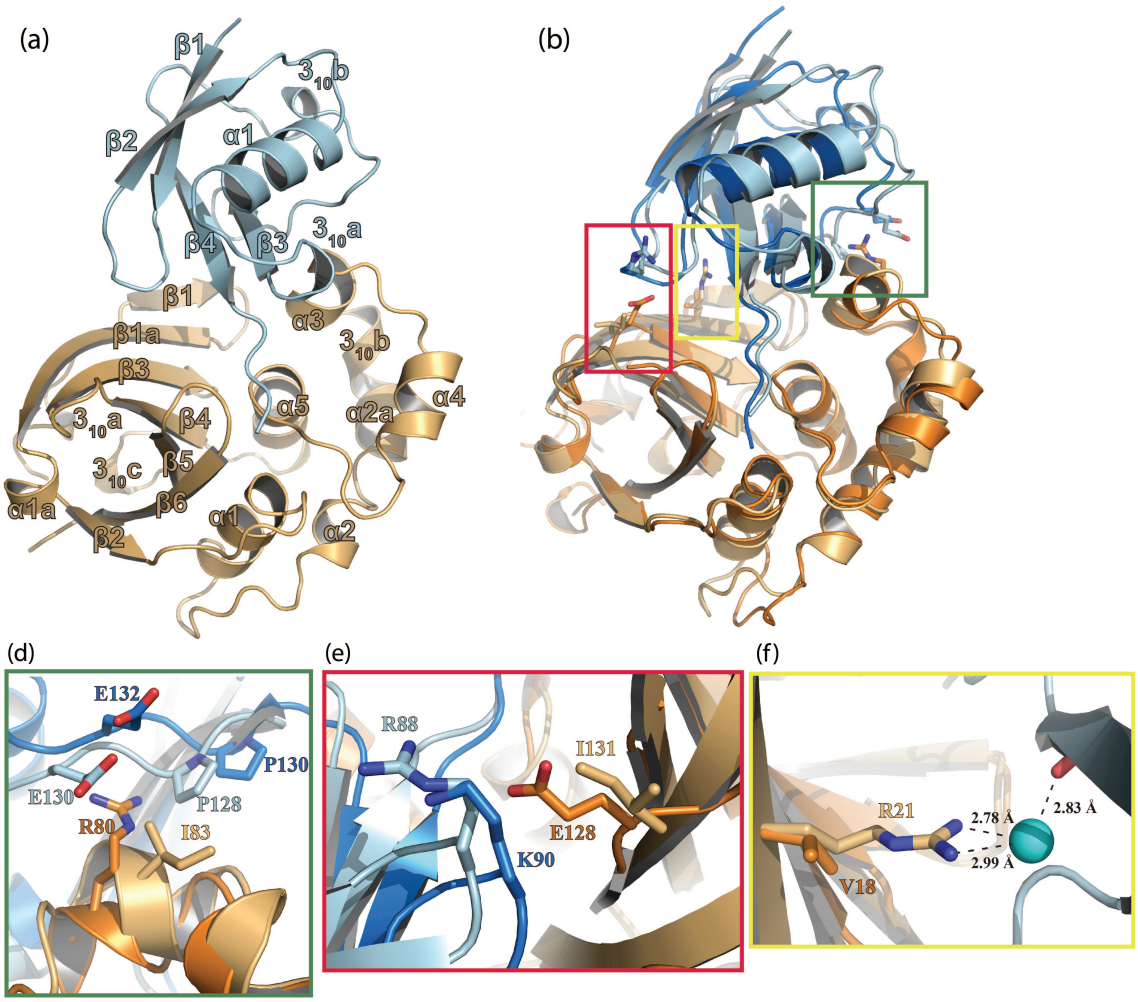

Figure 8: ERVEvOTU-CmISG15 crystal structure. (a) ERVEvOTU-CmISG15 crystal structure with ERVE vOTU rendered in light orange, and mISG15 in light blue. (b) Comparison of CCHFvOTU-ChISG15 (PDB entry 3PHX) with ERVEvOTU-CmISG15. ERVEvOTU-CmISG15 is rendered as in (a), CCHF vOTU is rendered orange, and ChISG15 is blue. Boxed in green is shown in detail in (d), boxed in red is shown in (e), and boxed in yellow is shown in (f). (d) Comparison of the α3 helix-binding interface between CCHFvOTU-ChISG15 and EVREvOTU-CmISG15, colored as in (b). (e) β-sheet / substrate binding interface of CCHF vOTU E128 with hISG15 K90, colored as in (b). (f) ERVE vOTU R21 H-bonding with CmISG15 backbone through coordinated water molecule, which is represented as a cyan sphere, while proteins are colored as in (b).

accommodated by the vOTU on the other side of the binding pocket in the β-sheet / substrate interface. Specifically, CCHF vOTU's E128, which faces into the binding pocket, interacts with the hISG15 K90 (Fig. 8e). By comparison, ERVE vOTU's

corresponding I131 does not favorably interact with either hISG15 or mISG15 in that location, and its mISG15 substrate is shifted away from this residue. To compensate, in another area of the binding pocket, ERVE vOTUs R21 can hydrogen bond with the carbonyl backbone of mISG15 through a coordinated water molecule, where CCHF vOTU's V18 is not favorably interacting with hISG15 (Fig. 8f).

Inhibition of CCHFvOTU by Mutants of CmISG15

Upon examination of ERVEvOTU-CmISG15 overlaid with CCHFvOTU-ChISG15, key areas were identified as possible recognition sites for ERVEvOTU's accommodation of both mISG15 and hISG15. While CCHF vOTU mutants V18R and E128I both significantly decreased in activity towards hISG15-AMC by approximately 50 and 60%, respectively, neither mutation made appreciable gains in recognition of CmISG15 by CCHF vOTU (Fig. 9).

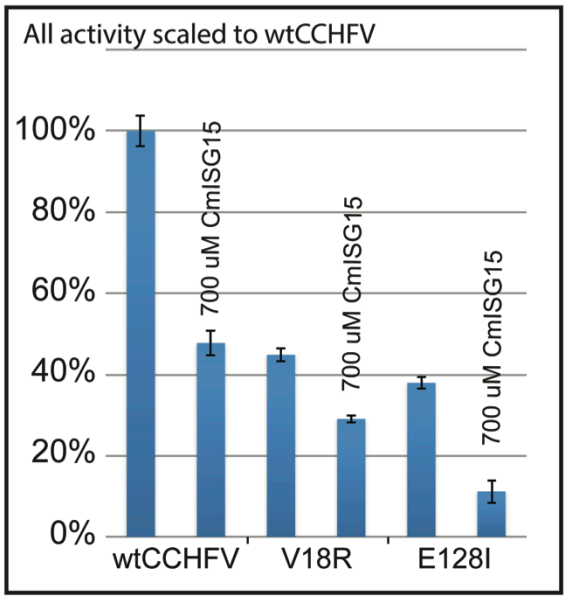

Figure 9: CCHF vOTU mutants inhibition by CmISG15.

ProISG15 Gel Shift Assay

In order to further explore the degree of species preference of varying nairovirus vOTUs, special constructs of ISG15 from human, sheep, northern tree shrew, and jackknife fish (hproISG15, sheep-proISG15, Nshrew-proISG15, and fish-proISG15, respectively) were designed with additional amino acids on the C-terminus. These amino acids are the sequence found on the pro-form on hISG15, plus a His-tag. By eliminating variation in this extension of the substrate, variation in the vOTUs' preference for these ISG15s could be investigated. CCHF vOTU readily cleaved the hproISG15 to completion within about 10 minutes (Fig. 10). Interestingly, it also cleaved the sheep-proISG15 and Nshrew-proISG15 rapidly, and after an extended time, 30-60 minutes, had cleaved a small amount of fish-proISG15. ERVE vOTU completely cleaved the hproISG15 within about 60 minutes, had about equal cleavage for the sheep-proISG15, a trace of activity toward fish-proISG15, but possessed zero activity toward the Nshrew-proISG15, even after 60 minutes. NSD vOTU cleaved both hproISG15 and NShrew-proISG15 completely after 30 minutes, and showed zero activity toward fish-proISG15. Interestingly, it rapidly cleaved the sheep-proISG15 within about 5 minutes. In contrast to the vOTUs, SARS PLpro was also paneled against the pro-ISG15 constructs. SARS PLpro exhibited moderate cleavage of hproISG15, leaving a trace amount uncleaved after 60 minutes, cleaved the sheep- and Nshrew-proISG15s within about 10 minutes, and was the DUB which exhibited the most activity toward fish-proISG15, cleaving about 40% within 60 minutes (Fig. 10). While SARS PLpro was more robust than the vOTUs towards the fish-proISG15, it still displayed preference for human, N. shrew, and sheep.

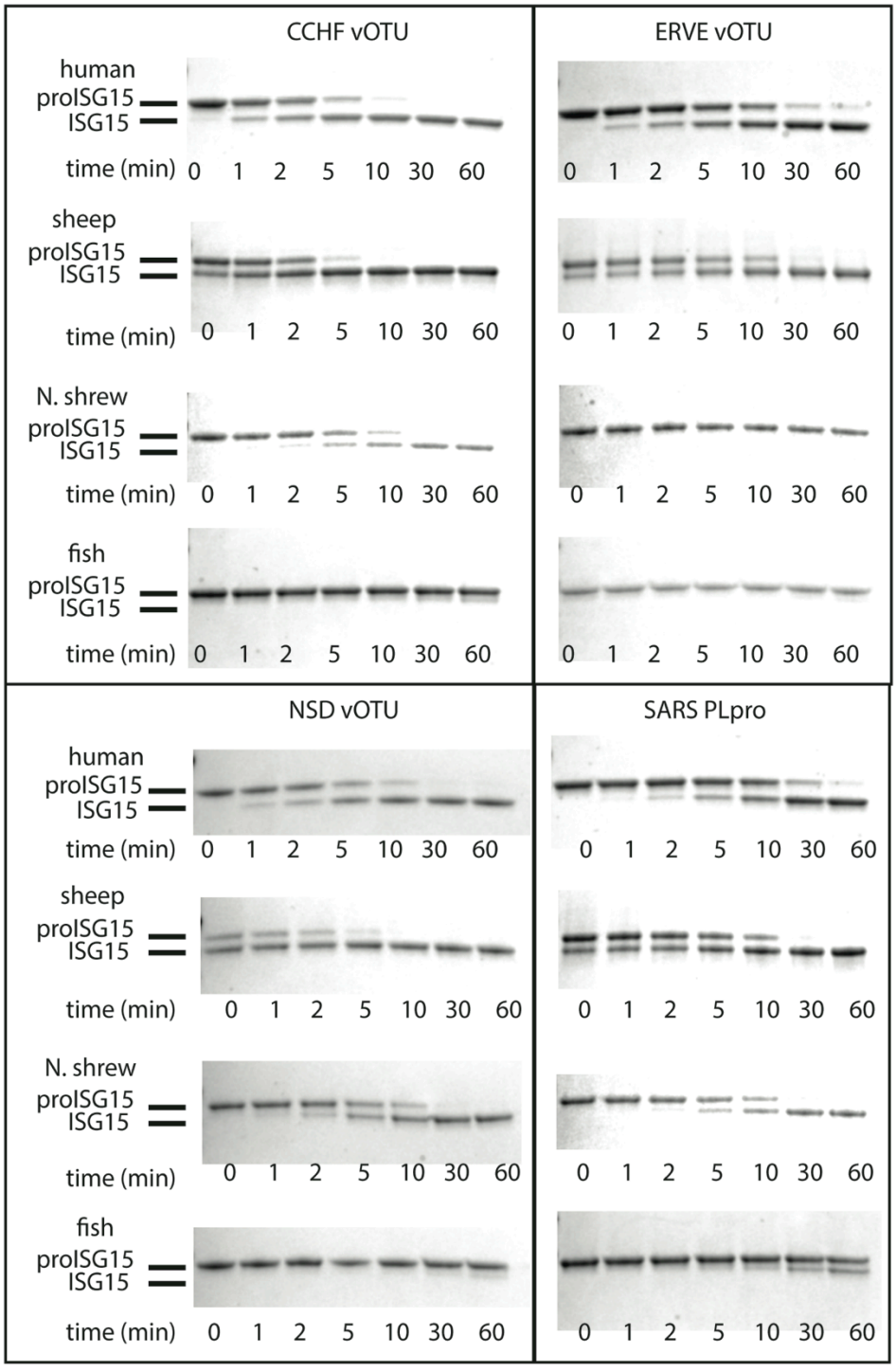

Figure 10: ProISG15 Gel Shift Assay. CCHF, ERVE, or NSD vOTU, plus SARS PLpro were evaluated for cleavage of human, sheep, N.shrew, and fish proISG15.

Discussion

Primary Structure Determinant of Substrate Preference

In Capodagli et al. (2013), it was determined that the primary structure of the CCHF and DUG vOTUs were key factors in substrate preference, and that global secondary and tertiary structural features were mainly conserved, with the minor exception of a shift of the α3-helix. In a similar manner, ERVE vOTU possesses conserved global folds of other nairovirus vOTUs, with a shift in the α3-helix similar to DUG vOTU. Ultimately, while the primary structure appears to be the driving force in determining substrate recognition, it results in slight shifting of the substrate within the binding pocket. This shift appears to accommodate varying substrates by balancing favorable contacts in different area of the binding pocket, specifically balancing favorable amino acid interactions on the binding interface between the β-sheet and substrate interface on the opposite side of the binding pocket as the α3-helix (Fig. 11). These slight adjustments of the substrate within the binding pocket allow the vOTUs to possess their dual activities towards varying substrates. While others have identified specific amino acid residues which can modulate the activity of CCHF or DUG vOTU toward Ub or ISG15 (James et al. 2011, Akutsu et al. 2011, Capodagli et al. 2013), there do not appear to be global control switches for Ub and ISG15 activity, but rather a collection of variations to the binding interfaces which have individually evolved for each vOTU. Furthermore, this shifting of substrate within the binding pocket may ultimately be what allows vOTUs to appear to possess activity towards substrates to which they could not have had evolutionary pressure to develop activity towards, as is the case with Turnip

Yellow Mosaic Virus (TYMV) as shown by Capodagli et al. (2013), which can be shown, at sufficiently high concentrations, to cleave hISG15-AMC, which is not known to exist in plants. Along a similar line, CCHF vOTUs lack of recognition towards mISG15 creates inherent problems for any mouse model systems for study of CCHFV. Under biologically relevant conditions, CCHF vOTU does not possess sufficient recognition of mISG15 to interfere with its role in viral immune response in mice.

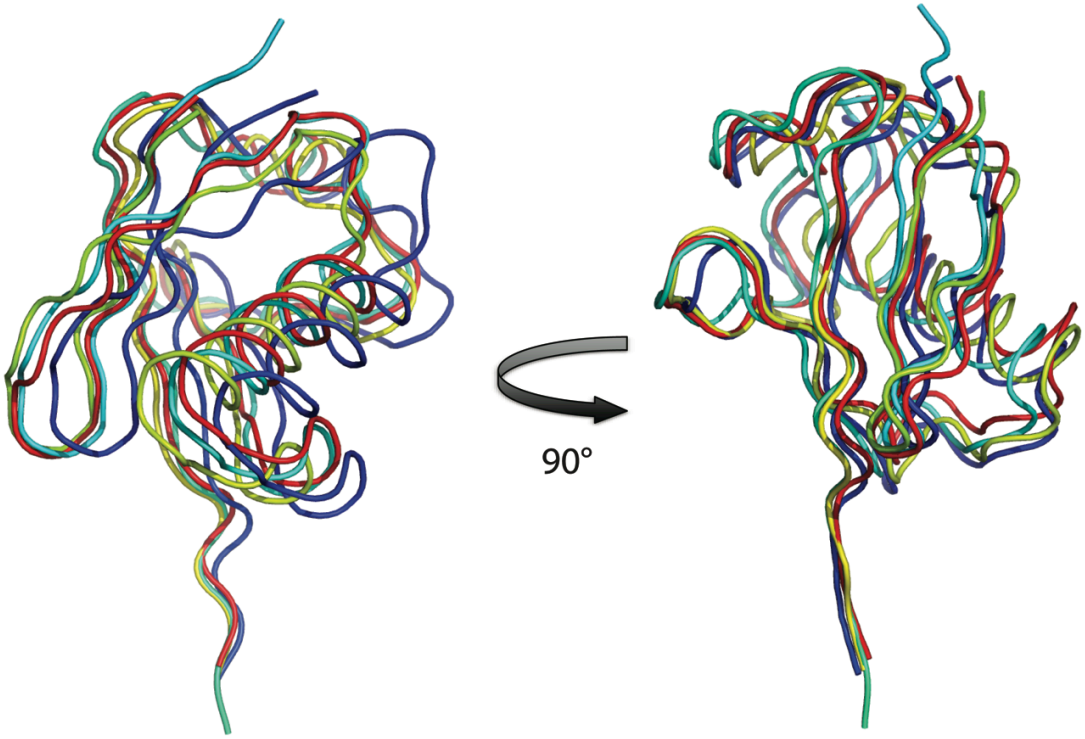

Figure 11: Comparison of Ub and ISG15 bound by CCHF vOTU, ERVE vOTU and DUG vOTU. the vOTUs from CCHFvOTU-Ub (PDB ID: 3PRP), DUGvOTU-Ub (PDB ID: 4HXD), CCHFvOTU-ChISG15 (PDB ID: 3PHX), and ERVEvOTU-CmISG15 were structurally aligned using SSM Superpose, and the resulting overlay of their respective substrates is shown. Ub bound to CCHF vOTU is shown green, Ub bound to DUG vOTU is red, ChISG15 bound to CCHF vOTU is cyan, and CmISG15 bound to ERVE vOTU is blue.

Diversity of ISG15 Recognition

Based on the inability of mISG15 to inhibit CCHF vOTU, it was hypothesized that CCHF vOTU was a more selective vOTU than ERVE vOTU, with a high specificity towards hISG15. The proISG15 gel shift assay revealed that CCHF vOTU can, in fact, cleave a variety of species' ISG15s. CCHF vOTU's high activity towards hISG15 and NSDV's strong preference and activity toward sheep ISG15 are in line with the role of the vOTU as a virulence factor through targeting ISG15 in species resulting in a high mortality rate. However, while a high activity toward ISG15 may be an indicator for virulence, it alone cannot explain why CCHFV is only found to be lethal in humans, when it also readily cleaves sheep and shrew ISG15. While the activity of the vOTU has been identified as one potential virulence factor, it is apparent that there are other factors, which have yet to be identified, that may work in concert with the robust vOTU deISGylation to result in high mortality for specific species.

Intriguingly, ERVE vOTU, which was inhibited by mISG15, and also readily cleaves sheep and human proISG15s, had no measurable activity towards the Northern shrew's ISG15. While ERVEV was isolated from the white-toothed shrew, this may represent another possible outcome of mutations that favor one substrate, such as Ub, or to become specific to one species' substrate, such as ISG15, when balancing competing factors affecting the vOTUs substrates preferences, and still maintaining necessary proteolytic activity for viral polypeptide processing. Favoring one role over another may cause a loss in activity for one and gains for another. Alternatively, in the possible

absence of a strong IFN response to infection by ERVEV in shrew, there may not be pressure for the ERVEV to develop activity toward the shrew's ISG15.

Including SARS PLpro in the panel of DUBs cleaving proISG15 constructs provides insight into the behavior of a different class of DUB. SARS PLpro has been shown to be a di-distributive DUB, preferentially cleaving K48 linked poly-UB, leaving behind mono-Ub on substrates (Ratia et al. 2014). While it cleaved all of the ISG15s paneled, it may be less driven by primary structure, as is seen with the vOTUs, and more by tertiary structural folds. It was seen by Ratia et al. (2014) that its specificity toward K48 poly-Ub over K63 poly-Ub was driven by a secondary binding site which accommodated K48 over the linear, K63 linkage, with the more condensed, bent structure of K48 nested into both its proximal and distal binding sites. It may be that the flexibility of the middle, hinge region of ISG15s allow them to conform to fit in the binding site of SARS PLpro. While only the C-terminal lobe of ISG15 is involved in binding to vOTU active sites, based on the manner in which K48 Di-Ub is proposed to fit into the SARS PLpro active site, it is likely that both lobes of ISG15 are involved in binding to SARS PLpro.

Implications for Mouse Model Systems

The elucidation of the x-ray structure of CmISG15 not only provides the first structural information for mISG15, but opens the door for further developing methods for potentially utilizing mouse model systems for study of viruses which express vOTUs, such as CCHFV. Current studies have demonstrated how to turn on and off specific substrate activities through mutation of select amino acids. Based on the findings that the

primary structure is key in dictating substrate selectivity, it is plausible that a hybrid vOTU could be developed which possesses robust activity towards mISG15, which could be investigated for a mouse model system for the development of therapeutics for CCHFV.

CHAPTER THREE: STRUCTURAL AND BIOCHEMICAL CHARACTERIZATION OF HUMAN ADENYLOSUCCINATE LYASE (ADSL) AND THE R303C ADSL DEFICIENCY ASSOCIATED MUTATION

Introduction

Adenylosuccinate lyase (ADSL) deficiency is a rare autosomal recessive disorder characterized by serious neurological and physiological symptoms such as psychomotor retardation (PMR), expression of autistic features, structural brain abnormalities, axial hypotonia, seizures, peripheral hypotonicity, ataxia, muscle wasting, growth retardation and strabismus (Spiegel, Colman, and Patterson 2006, Mouchegh et al. 2007, Gitiaux et al. 2009). More than 60 cases of ADSL deficiency have been reported worldwide, but it is widely considered to be underdiagnosed (Köhler et al. 1999, Jurecka et al. 2008, Ciardo, Salerno, and Curatolo 2001). ADSL deficiency is clinically diagnosed by elevated levels of succinylaminoimidazolecarboxamide riboside (SAICAr) and succinyladenosine (S-Ado) in urine, plasma, and cerebrospinal fluid (Georges and Berghe 1984). Three distinct phenotypic groups have been established: 1) Neonatal; 2) Type I; 3) Type II. The neonatal form results in fatal neonatal encephalopathy and has a S-Ado:SAICAr ratio of <1. Type I patients experience early onset, severe PMR, and have a ratio of ~1. Type II patients experience later onset with mild PMR, and have a ratio of 2–4 (Van den Bergh, Vincent, Jaeken, and Berghe 1993). There are three main hypotheses that describe the difference in ratio: 1) nonparallel reduction in the enzyme's activity on

its substrates; 2) differential dephosphorylation or transport of the substrates out of the cells (Van den Bergh, Vincent, Jaeken, and Berghe 1993, Hürlimann et al. 2011), and 3) inability of ADSL mutant protein to form an active purinosome, which is formed when purine synthesis is required and is needed for appropriate channeling of succinylaminoimidazolecarboxamide ribonucleotide (SAICAR) through the *de novo* purine synthesis pathway (Baresova et al. 2012). ADSL carries out two non-sequential steps of *de novo* AMP synthesis, the conversion of SAICAR and succinyladenosine monophosphate (SAMP) into aminoimidazolecarboxamide ribotide (AICAR) and adenosine monophosphate (AMP), respectively, with the concomitant release of fumarate in each case (Lundy et al. 2010). The conversion of SAMP to AMP is also part of the purine nucleotide cycle. So far, all mutations, with one exception, result in a proportional loss of enzyme activity with the two substrates. The ADSL carrying the R303C mutation has been observed as a homozygous mutation in two unrelated patients. It is a type II mutation and results in the mildest observed form of ADSL deficiency. Interestingly, this mutation shows a more severe loss in activity with SAMP than with SAICAR, although the extent of disproportionality varies from study to study, perhaps reflecting differences in how the enzyme assays were carried out. Some investigators were unable to detect activity with SAMP in extracts from fibroblasts (Race et al. 2000), while others found 3% of normal activity (Van den Bergh, Vincent, Jaeken, and Berghe 1993). In other cases using different recombinant ADSL constructs, 7% and 18 % of wild-type (WT) activity was observed with SAMP and 44% with SAICAR (Race et al. 2000, Zikánová et al. 2010). The reason for the non-parallel loss of activity is not yet understood, nor is the

reason why this mutation leads to such a mild phenotype. Hypotheses include the possibility that different amino acids in the active site bind the two substrates, that cysteine is not able to interact well with SAMP, or that there are alterations in the stability of the active site cleft (Race et al. 2000, Zikánová et al. 2010). Crystal structures of the bacterial ADSL and other studies have provided insight into the active site and the catalytic mechanism; however these studies predominately use bacterial ADSL from organisms such as *Thermotoga maritima* or *Escherichia coli* (Toth et al. 2000, Tsai et al. 2007). *T. maritima* and *Homo sapiens* have a sequence identity of 25% and similarity of 57%. *E. coli* and *H. sapiens* have a sequence identity of 23% and a similarity of 57% (Fig. 12). ADSL was found in these bacterial species to function in the pathway as a homotetramer. Interestingly, three monomers contribute to each of the four active sites in the tetramer (Sivendran and Colman 2008, Brosius and Colman 2002). The use of *Bacillus subtilis* ADSL in particular as a model to study properties of mutant enzymes in some cases involved modification of additional amino acid residues in the *B. subtilis* ADSL to more closely resemble human ADSL (Sivendran et al. 2004, Palenchar and Colman 2003). However, attempts to make use of a *B. subtilis* model system to replicate the R303C phenomenon have proven difficult because *B. subtilis* and *H. sapiens* only have a sequence identity of 30% and a similarity of 63%. Specifically, the sequence diversity of *B. subtilis* and *H. sapiens* results in multiple alterations within the active site including, but not limited to, an asparagine residue in place of the corresponding R303 in human ADSL, as well as an arginine residue in place of human corresponding T354. Not surprisingly, the removal of *B. subtilis*'s asparagines at the corresponding human ADSL

R303 position for cysteine did not generate a disproportional reduction in catalytic ability (Palenchar and Colman 2003, Sivendran et al. 2004). This observation as well as others suggest that the study of the bacterial enzyme, while initially useful for understanding some of the basic features of ADSL, such as its tetrameric nature and participation of three subunits in forming each active site, may not be as useful for understanding the effects of various disease causing mutations on the human enzyme. Only limited structural information exists of human ADSL active site in the unpublished SAMP bound and S-AMP/AMP-fumarate bound PDB deposited entries (2J91, 2VD6). Current studies on disease-associated mutations of human ADSL have focused on correlation of substrate activity with clinical phenotypes, thermal stability of ADSL, activity of hybrid WT ADSL and mutants, and global changes in structure (Zikánová et al. 2010, Ariyananda et al. 2011, Ariyananda et al. 2009, Race et al. 2000, Kmoch et al. 2000). They have not investigated local structural changes or binding properties to the products within the ADSL active site. In this study, we present structural and biochemical characterization data of WT and mutant R303C ADSL by enzyme kinetics, product binding by isothermal titration calorimetry (ITC), and X-ray crystallography to reveal the effects of the R303C mutation that results in nonparallel reduction in enzyme activity.

Experimental Procedures

Materials

Chemicals, biochemicals, buffers, and solvents were purchased from Sigma-Aldrich Chemical Co. (St. Louis, MO), Fisher Scientific Inc. (Pittsburgh, PA), Fluka Chemical Corp. (Milwaukee, WI), or EM Science (Cincinnati, OH). The Centricon and

Ultrafree centrifugal filter devices were obtained from Millipore Co. (Billerica, MA). Nickel-nitrilotriacetic acid-agarose, a QIAspin kit, and high throughput crystal condition screens were purchased from QIAGEN. Additive HT Screen was purchased from Hampton Research. QuikChange site directed mutagenesis kit was purchased from Stratagene. SAICAR was prepared enzymatically from AICAR purchased from Sigma-Aldrich Chemical Co. as described by Zikánová et al. (2005). Enzymes and reagents used for molecular biology procedures were obtained from New England Biolabs, Inc. (Ipswich, MA).

Site-directed mutagenesis, Enzyme Expression, and Purification.

The initial WT ADSL construct was obtained from Dr. Roberta F. Colman, Department of Chemistry and Biochemistry, University of Delaware, Newark, DE. The full description of the initial WT ADSL construct is described in Lee and Colman (2007). In short, the full length human ADSL gene (1-484 residues) was constructed in pET-14b vector containing a 5'end *Nde*I restriction site and a 3'-end *Blp*I restriction site and a thrombin cleavable N-terminal histidine tag. In order to overexpress the human enzyme in *E. coli*, the vector was transformed into *E. coli* Rosetta 2(DE3)pLysS. The WT and R303C ADSL were purified to homogeneity using a Qiagen Ni-NTA column. Purity was assessed by SDS-PAGE gel electrophoresis (data not shown). After purification, protein was stored in Enzyme Storage Buffer (50 mM potassium phosphate buffer, pH 7.0, containing 150 mM KCl, 1 mM DTT, 1 mM EDTA, and 10% (v/v) glycerol) at -80°C. Introduction of point mutations in the human ADSL plasmid was done using QuikChange site-directed mutagenesis. The QIAspin kit was used for cDNA extraction and

purification. DNA sequencing was performed at the CU Cancer Center DNA Sequencing & Analysis Core to confirm mutations. Slight modifications were made to the purification for ITC and X-ray Crystallography. Following the purification using the Qiagen Ni-NTA column, thrombin was added to the eluted fraction and it was dialyzed overnight at 4°C in ADSL Running Buffer (5 mM HEPES pH 7.0, 150 mM KCl, 2 mM DTT) to cleave the His-tag. The protein was purified by size exclusion chromatography using S200 sepharose resin and concentrated to 10 mg/mL for crystallography, and to 200-400 μM for ITC. Concentrations were measured by the absorbance at 280 nm using an experimentally determined extinction coefficient of 0.782 L $g^{-1}cm^{-1}$ (43,150 $M^{-1}cm^{-1}$) for thrombin cleaved ADSL and 0.770 L $g^{-1}cm^{-1}$ for His-tagged ADSL following previously established procedures (Gill and von Hippel 1989).

Static Light Scattering

Size Exclusion Chromatography-Multi-Angle Light Scattering measurements were performed on a Wyatt miniDAWN TREOS connected to a Shimadzu UFLC and a Wyatt WTC-030S5 size exclusion column. Samples of 350 μg of His-tagged ADSL diluted in Enzyme Storage buffer were run in duplicate. PBS was used as the mobile phase and flowed at 0.5 mL/min. Calibration was checked using 2 mg/mL bovine serum albumin. Data were analyzed with ASTRA software, and 0.185 was used as the dn/dc value.

Enzyme Assays and Kinetic Studies

Enzyme kinetic experiments were performed on a UV-Vis Spectrophotometer Evolution 3000 from Thermo Scientific using 1 mL quartz cuvettes at 25°C. ADSL with

the His-tag intact was used for enzyme assays, as it has been shown that the His-tag does not affect ADSL activity for SAMP (Lee and Colman 2007). Experiments were run with concentrations of 0.11 mg/mL and 0.19 mg/mL for WT and R303C ADSL, respectively. Frozen samples were incubated for ~2 hours at 25°C before measurements were taken to assure restoration of full activity (Lee and Colman 2007). SAMP enzyme assays of ADSL were measured in triplicate at 25°C in 40 mM Tris-HCl (pH 7.4) with varying concentrations of SAMP (1 - 60 μM). Specific activity was measured from the decrease in absorbance of SAMP at 282 nm as it was converted to AMP and fumarate. The assay was monitored over 30 seconds in a 1 mL volume. The difference in extinction coefficient of 10,000 M^{-1} cm^{-1} between SAMP and AMP was used to calculate the specific activity. SAICAR enzyme assays of ADSL were measured in triplicate at 25°C in 40 mM Tris-HCl (pH 7.4) with varying concentrations of SAICAR (1 - 100 μM). Specific activity was measured from the decrease in absorbance of SAICAR at 269 nm as it was converted to AICAR and fumarate. The assay was monitored over 30 seconds in a 1 mL volume. The difference in extinction coefficient of 700 M^{-1} cm^{-1} between SAICAR and AICAR was used to calculate the specific activity. To determine the kinetic constants, the initial velocity data were fitted to the Hill equation, $\upsilon = V_{max}*[S]^n/(K_{0.5}{}^n+[S]^n)$ for WT and R303C ADSL and $\upsilon = V_{max}*[S]/(K_M+[S])$ for R303C ADSL, using the Enzyme Kinetics Module 1.3 of Sigma Plot version 10 (SPSS Inc.). The k_{cat} value was calculated from V_{max} and the enzyme concentration [E] via the equation $k_{cat} = V_{max}/[E]$.

Isothermal Titrations Calorimetry (ITC)

ITC experiments were conducted using a NANO-ITC system (TA Instruments, Utah, USA). Thrombin cleaved WT ADSL was dialyzed overnight against a solution of 25 mM HEPES pH 7.0, 150 mM KCl, and 2 mM DTT. AMP was brought to a concentration of 2.5 mM using the buffer in which WT ADSL was dialyzed. ITC runs of WT ADSL with AMP were performed in duplicate and comprised of a single 1μl injection followed by 24, 2 μl injections for a total of 25 injections of 2.5 mM AMP into 0.250 mM WT ADSL. Each injection was spaced 250 seconds apart. ITC experiments were performed in an identical method, injecting AICAR instead of AMP into 0.225 mM WT ADSL. In addition, AMP and AICAR were titrated in an equal manner into 0.280 mM R303C ADSL. Data sets were analyzed with NanoAnalyze software and fit to an independent model concurrently with a blank constant model to adjust for heat of dilution.

Crystallization of WT and R303C ADSL

Initial crystal conditions for both WT and R303C ADSL were determined from high-throughput screening of Qiagen Nextel screens, Classics and PEG I, in a 96 sitting drop format using an Art Robbins Phoenix robot. The drops consisted of 0.4 μL protein solutions and 0.4 μL precipitate in a 100 μL reservoir. Initial screening exhibited multiple hits; however, a solution containing 0.1 M Tris pH 8.0, and 20% (w/v) PEG 6000 produced the most viable crystals for WT ADSL, and 0.1 M Tris pH 8.5 and 20% (w/v) PEG 8000 for the ADSL mutant R303C. These crystals were then optimized using Additive HT Screen from Hampton Research. Final WT and R303C ADSL crystals were

obtained through vapor diffusion using a 500 µL reservoir with 4 µL drops mixed 1:1 with protein solution and, for native ADSL, a precipitant gradient of 18-28% (w/v) PEG 6000, 0.1 M Tris pH 8.0, and 12.5 mM $MgCl_2 \bullet 6H_2O$, and for R303C, a precipitant gradient of 18-28% (w/v) PEG 8000, 0.1 M Tris pH 8.5, and 12.5 mM spermine tetrahydrochloride.

X-ray Structural Determination of ADSL Structures

All X-ray native datasets were collected using crystals mounted on nylon loops and submerged in a 5 µL cryo solution of 26% (w/v) PEG 6000 and 0.1 M Tris pH 8.0 for WT ADSL, and 26% (w/v) PEG 8000, 0.1 M Tris pH 8.5 for R303C ADSL. In order to preserve the crystals they were submerged and flash frozen in liquid nitrogen. Frozen crystals were mounted under a stream of dry N_2 at 100 K. A WT ADSL dataset with resolution to 2.70 Å and ADSL mutant R303C dataset with resolution to 2.60 Å were collected at the 21-ID-D Life Science-Collaborative Access Team beamline at the Advanced Photon Source Synchrotron. Both datasets were collected at 0.9789 Å with a MarMosaic300 CCD detector (Rayonix). All data was subsequently processed and scaled using Scalepack (Winn et al. 2011) and subsequent phases were determined and refined using Phaser (McCoy et al. 2007). Initial models for both WT and R303C ADSL were elucidated by molecular replacement using ADSL structure 2J91 as a search model for Phaser (McCoy et al. 2007). Both structures were refined using iterative cycles of model building and structure refinement using WinCOOT (Emsley and Cowtan 2004) and REFMAC (Murshudov, Vagin, and Dodson 1997), respectively. Water molecules were added to 2*Fo-Fc* density peaks that were greater than 1σ using the "Find Water"

WinCOOT program function. The final model was checked for structural quality using the CCP4 suite programs: Procheck and Sfcheck. Data processing and refinement statistics are shown in Table 2.

Table 2: Data Collection and Refinement Statistics ADSL

	WT APO	R303C ADSL
Data Collection		
Space Group	$P2_12_12_1$	$P2_12_12_1$
Unit Cell Dimensions		
a, b, c (Å)	85.9, 105.1, 215.0	85.8, 105.6, 217.2
α=β=γ (degrees)	90.0, 90.0, 90.0	90.0, 90.0, 90.0
Resolution (Å)	50.0-2.70	50.0-2.60
No. Reflections Observed	241,786	263,513
No. Unique Reflections	48,725	58,820
Rmerge (%)	10.3 (63.1)*	12.4 (35.0)*
I/σI	14.2 (4.3)*	18.9 (4.8)*
% Completeness	89.6 (90.2)*	95.4 (97.1)*
Refinement		
Resolution Range	50.0-2.70	50.0-2.60
No. Reflections in Working Set	45,972	55,609
No. Reflections in Test Set	2,450	2,979
Rwork (%)	24.3	23.0
Rfree (%)	29.2	29.8
Mean B-factor ($Å^2$)	27.5	55.1
Protein B-factor ($Å^2$)	27.6	54.9
Water B-factor ($Å^2$)	19.2	50.1
RMS deviation:		
Bond Lengths (Å)	0.01	0.01
Bond Angles (degrees)	0.9	1.01
Protein / Water Atoms	14,605/214	14,764/144
Monomers in Asymmetric Unit	4	4

* The last resolution shell is shown in parentheses.

a Rmerge=$\Sigma h \Sigma i |Ii(h) - \langle I(h) \rangle| / \Sigma h \Sigma i Ii(h)$, where Ii(h) is the ith measurement and $\langle I(h) \rangle$ is the weighted mean of all measurements of I(h).

b Rwork and Rfree=$h(|F(h)o| - |F(h)c|)/h|F(h)o|$ for reflections in the working and test sets.

Modeling of AMP/AICAR and Fumarate Binding in the Active Site

Apo structures of WT ADSL with either AICAR or AMP were neutralized with the TLEAP module from the Amber10 simulation package (Pearlman et al. 1995, Case et al. 2005) and solvated using TIP3P water molecules (Jorgensen et al. 1983). The final system was then energy minimized using the Amber 10 simulation package to obtain the final structure. Initially, each system's protein was restrained, and the solvent was minimized for 5,000 steps to remove any unfavorable contacts that occurred within the water. Then, each system (solvent and molecule) was allowed to energy minimize for 20,000 steps, starting with 10,000 steps of steepest descent and switching to 10,000 more steps of conjugate gradient minimization. The force field used was ff99SB (Hornak et al. 2006). We removed residues outside of 30 Å from AMP/AICAR active site. This was done to reduce computational demand by ignoring distant parts of the protein not relevant for the present problem. However, 30 Å was long enough to focus on a sufficiently large region around the active site to avoid any artifact due to small system size. All the calculations were performed at University of Denver's High Performance Computing facility, which is a Linux cluster with 22 twin nodes, each node having eight cores.

Results

WT and R303C ADSL Enzyme Kinetics

To ensure that the previously observed reduction in activity of the ADSL possessing the R303C mutation was not due to aberrant tetramer formation or outright global instability of the mutated protein in solution, static light scattering was employed to determine the polymeric distribution of the R303C and WT ADSL. As expected, WT

ADSL is predominantly found to be a tetramer, 92.7 ± 2.6%, with aggregates contributing the final percentage. Similarly, R303C ADSL is predominantly a tetramer, 94.3 ± 0.1%, with aggregates contributing the final percentage. Observed weights of the WT and R303C ADSL tetramers were 225.0 ± 2.9 kDa and 214.5 ± 12.2 kDa, which is in close agreement with the His-tagged WT and R303C ADSL predicted tetrameric weights of 228.4 and 228.1 kDa, respectively, suggesting that the R303C mutation results in no degradation of the ADSL tetramer.

Previously, a report noted that the ADSL carrying the R303C mutation displayed nonparallel decrease in activity at a single concentration (Zikánová et al. 2010). Additionally, the kinetic parameters for human ADSL utilization of SAICAR have never been fully determined. Interestingly, Stone, Zalkin, and Dixon (1993) detail a K_M and k_{cat} of ADSL for SAICAR. Unfortunately, the boundaries of ADSL were not well established at the time of that study, resulting in their use of a 25 amino acid N-truncated version of ADSL and not accounting for cooperativity. Unfortunately, a subsequent study by Kmoch et al. (2000) also did not account for ADSL cooperativity, nor did they report on the R303C mutant. This has left ambiguity to the kinetic parameters surrounding ADSL ability to use SAICAR as a substrate. To further investigate the R303C phenomenon and determine the K_M and k_{cat} of ADSL for SAICAR, kinetic assays were performed on both WT and R303C ADSL using SAICAR and SAMP as substrates (Zikánová et al. 2010). Both WT and R303C ADSL had measurable activity that could be evaluated by monitoring the UV absorbance of either SAMP or SAICAR. As WT ADSL was previously reported not to follow simple Michaelis-Menten kinetics for SAMP and

perhaps be cooperative, the Hill equation was initially employed for calculating WT ADSL's kinetic parameters (Table 3) (Ariyananda et al. 2009). The resulting Hill coefficients of WT ADSL for SAMP and SAICAR are both significantly above one, indicating cooperativity for the substrates. The resulting k_{cat} and $K_{0.5}$ of WT ADSL for SAMP was in agreement with a prior study that utilized the non-truncated form of ADSL (Ariyananda et al. 2009). For WT ADSL's utilization of SAICAR, its $K_{0.5}$ was 1.8 ± 0.1 μM, which is only slightly higher than SAMP's. However, WT ADSL's k_{cat} for SAICAR was 1.6 fold higher than that for SAMP suggesting that ADSL is more kinetically efficient for the catalysis of SAICAR over SAMP. This is confirmed by WT ADSL's $k_{cat}/K_{0.5}$ for SAICAR being 2 fold higher than SAMP's. Additionally, the k_{cat} for both substrates was found not to be diffusion limited.

Table 3: Enzymatic Activities of ADSL with SAMP and SAICAR at 25 C

	SAMP		SAICAR	
	WT	R303C	WT	R303C
$k_{cat,H}$ (1/sec)	52.2 ± 1.8	2.33 ± 0.07	90.2 ± 1.9	27.8 ± 0.8
$k_{cat,H}$ (%)	100 ± 3	4.5 ± 0.1	100 ± 2	31 ± 1
$K_{0.5}$ (μM)	2.1 ± 0.2	2.3 ± 0.12	1.8 ± 0.1	8.4 ± 0.8
Hill Coeff	1.5 ± 0.2	1.03 ± 0.08	1.22 ± 0.09	0.94 ± 0.06
$k_{cat,H}/K_{0.5}$ ($sec^{-1}\mu M^{-1}$)	25.0	0.99	49.6	3.37
$k_{cat,M}$ (1/sec)	N/A	2.36 ± 0.04	N/A	27.2 ± 0.4
$k_{cat,M}$ (%)	N/A	4.5 ± 0.1	N/A	30 ± 1
K_M (μM)	N/A	2.4 ± 0.2	N/A	7.8 ± 0.4
$k_{cat,M}/K_M$ ($sec^{-1}\mu M^{-1}$)	N/A	0.99	N/A	3.45

The k_{cat}, $K_{0.5}$, K_M, and Hill coefficient were determined by varying substrate concentration and fitting data to the Hill Equation (H) or the Michaelis-Menten Equation (M) in Sigma Plot. Protein was reconstituted for 2 hours at 25 ^{o}C prior to measurements. R303C activity is relative to % WT. The values are shown along with their standard errors. N/A stands for not applicable.

Introduction of the R303C mutation into ADSL has multiple effects. Initially expecting similar cooperativity observed in WT ADSL, the Hill equation was utilized (Table 3). Unlike WT ADSL, the R303C ADSL demonstrates no cooperativity, with a Hill coefficient for both substrates of one. As a result, the simple Michaelis-Menten equation was employed for R303C. The R303C ADSL mutation reduces k_{cat} to 4.5% and 30% of that relative to WT ADSL for SAMP and SAICAR, respectively. Interestingly, this 7-fold difference in residual in vitro activity is in line with cell free extract studies of a Type II patient's fibroblasts carrying the R303C mutation, which had 3% of normal SAMP activity and 30% of normal SAICAR activity (Race et al. 2000, Van den Bergh, Vincent, Jaeken, and Van den Berghe 1993). As a result, the ratio of activity of WT ADSL for SAICAR:SAMP is 1.7, which is in agreement with a previously published ratio of 1.6, but the ratio of activity for the R303C mutant ADSL shifts to 11.5 (Ariyananda et al. 2011). Interestingly, K_M values of R303C ADSL increased for SAICAR compared to that of WT ADSL. The change observed in K_M of R303C ADSL for SAMP is almost negligible, with the K_M for SAICAR increasing more than 4-fold. This may initially suggest the mutation affects the ability of R303C ADSL to bind SAICAR more than SAMP resulting in the disparity in their cleavage. However, the rate of SAICAR cleavage by R303C ADSL is 5 times more rapid than that for SAMP at R303C ADSL's SAMP K_M. Therefore, the effect of the R303C mutation on ADSL may not solely be reflective in its divergent ability to bind SAICAR and SAMP. It suggests that R303C may affect the catalytic mechanism of SAMP and SAICAR in addition to binding of the substrates.

Isothermal Titration Calorimetry (ITC)

To explore the possible thermodynamic factors involved in the non-parallel reduction in activity resulting from the R303C mutation and in general ADSL-substrate interactions, ITC was performed on WT and R303C ADSL with their products AMP and AICAR. By measuring the amount of heat liberated per injection as a function of the molar ratio of the substrate and protein, thermodynamic parameters for R303C and WT ADSL's interaction with their products were calculated (Table 4). Intriguingly, product binding does not show any evidence of cooperativity, as the data fit to an independent model rather than a multiple binding site model. This does not necessarily rule out the possibility that the substrate binding is cooperative, but suggests that cooperativity may require inclusion of interactions between the fumarate component of the substrates and ADSL, which is lacking in the products.

Table 4: ITC Thermodynamic Parameters of ADSL

	AMP		AICAR	
	WT	R303C	WT	R303C
Kd (μM)	54 ± 3	130 ± 8	34 ± 2	121.9 ± 0.9
ΔH (kJ*mol^{-1})	-35 ± 2	-5.9 ± 0.2	-53 ± 1	-16.7 ± 0.5
TΔS (kJ*mol^{-1})	-12 ± 1	15.92 ± 0.06	-28 ± 1	5.3 ± 0.5
ΔG (kJ*mol^{-1})	-23.9 ± 0.1	-21.8 ± 0.2	-25.1 ± 0.1	-21.95 ± 0.02
n	0.99 ± 0.01	1.01 ± 0.04	1.00 ± 0.02	1.00 ± 0.02

Data sets were collected in duplicate and analyzed with NanoAnalyze software and fit to an independent model concurrently with a blank constant model to adjust for heat of dilution. All measurements were from 25 injections of 2.5 mM AMP into 170 μL protein in 25 mM HEPES, pH 7.0, 150 mM KCl, 2 mM DTT at 20°C.

Beyond the absence of cooperativity observed, the K_d values for WT ADSL were 54 and 34 μM for AMP and AICAR, respectively (Table 3). The thermodynamic properties that are responsible for AICAR and AMP binding to WT ADSL globally are

similar with the enthalpic component, ΔH, being the predominant driving force and the entropic component, ΔS, being unfavorable. Although similar, the thermodynamic properties are not identical. AICAR binding liberates an additional 18 kJ/mol, suggesting an additional hydrogen bond may be formed between AICAR and WT ADSL that is absent in an AMP and WT ADSL complex. The lack of this additional enthalpic contribution is partially offset in the AMP and WT ADSL complex by the reduced unfavorable entropic component compared to the AICAR and WT ADSL complex. Overall, this leads to a difference in ΔG of AMP and AICAR to WT ADSL to be only 1.2 kJ/mol in AICAR's favor.

Intriguingly, the R303C mutation impacts the ability of ADSL to form a complex with AMP and AICAR in two distinct manners. The enthalpic component for both products decreases by a similar degree of ~30 kJ/mol suggesting the loss of one to two hydrogen bonds, whose identity could be common between the two products and ADSL. Additionally, the R303C mutation shifts the ADSL complex formation with AMP and AICAR from an unfavorable to favorable entropic event. Taken together, these thermodynamic factors result in a similar decrease of ΔG and increases of 76 and 88 μM in the K_d of AMP and AICAR respectively. As a result, the R303C mutation appears to negatively affect ADSL's interaction with AMP and AICAR almost indistinguishably.

X-ray Structural Elucidation of R303C and WT ADSL

Recently, a study proposed that the R303C mutation may distort the active site cleft (Zikánová et al. 2010). To investigate the structural effects of the R303C mutation on ADSL and how these effects might be linked to the lower activity and unique

specificity of ADSL with the R303C mutation, the crystal structure of R303C ADSL (R303C-ADSL) was elucidated to 2.60 Å. A homo-tetramer in the asymmetrical unit was observed, with each monomer composed of 16 α -helices and 3 small β -sheets, which can be further divided into three domains (Fig. 12, 13). Electron density was observed for the majority of all 5–476 ADSL residues in all monomers, with residues 5–112 forming domain 1, residues 113–364 as domain 2, and 364–476 as domain 3. A notable exception was the residue range 286–291 in all monomers. These residues comprise the β3-α10 loop, also known as the C3 loop, which is located near ADSL's active site and expected to contain an important catalytic serine, S289. The lack of density for this region is not fully unexpected, as it has been unobserved in all but one bacterial ADSL X-ray structure. As a result, the loop is suggested to be highly flexible. Apart from the expected differences in the positions of the residues just prior to and after the missing density of the β3-α10 loop, the only other notable difference observed between the four monomers of R303C-ADSL resides in domain 3 of the structure. This domain is on the periphery of the tetrameric complex likely resulting in the small alterations and higher B-factors between the four monomers in that region (Fig. 13).

Despite these differences on the periphery of the protein, from a distance the R303C-ADSL globally resembles that of the PDB entry 2VD6 ADSL with its four active sites a mixture of active site bound SAMP, or AMP with fumarate (ADSL-SAMP) as well as AMP bound ADSL PDB entry 2J91 (ADSL-AMP). Unlike ADSL-AMP where

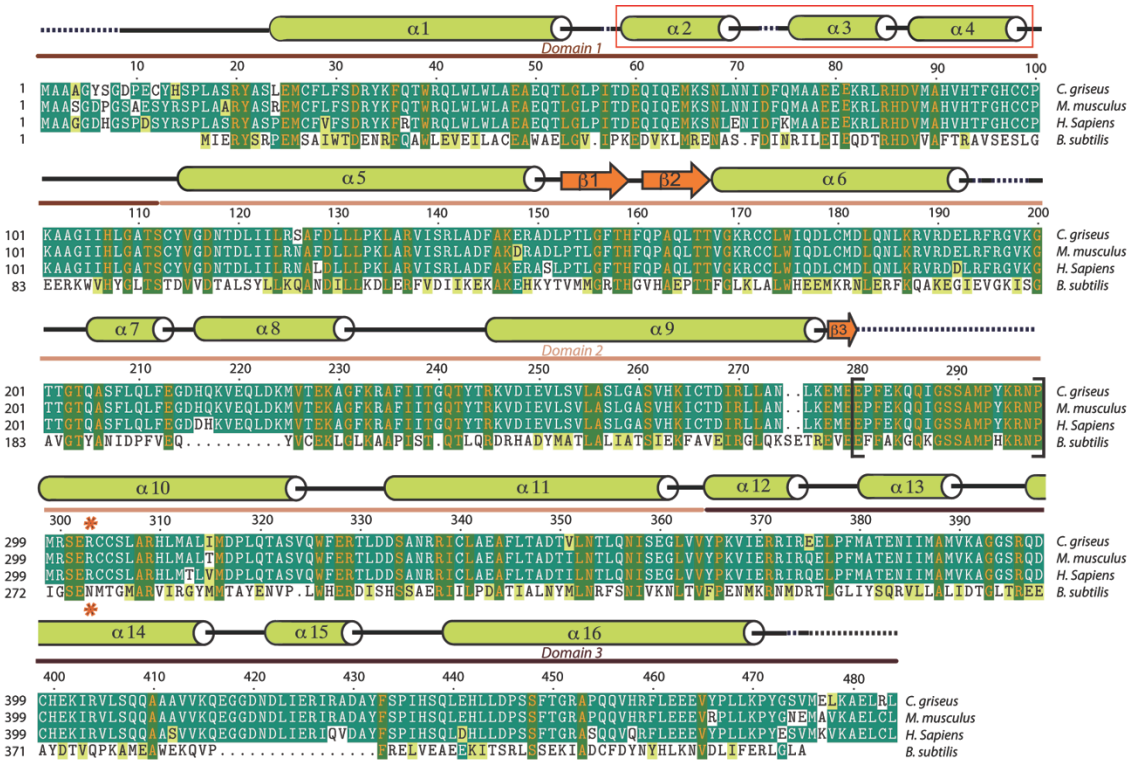

Figure 12: Sequence alignment of ADSL from various species. ADSLs are from *H. sapiens* (GenBank AAC83935.1), *M. musculus* (GenBank AAB60684.1), *B. subtilis* (NCBI Reference Sequence: YP_003865018.1), and *C. griseus* (NCBI Reference Sequence: NP_001230974.1). Secondary structure of hADSL according to Defined Secondary Structure of Proteins (DSSP) is represented by green cylinders (helical regions), orange arrows (β-sheet regions), black lines (loops), and black dashes (unstructured regions). Mutation site 303 is marked with an asterisk. The location of helices α3 and α4 is highlighted with a red box. The C3 loop is enclosed in black brackets. Catalytic residues H159 and S289 are marked with blue asterisks. Domains 1, 2, and 3 are indicated with bars in shades of brown.

all of the active sites are indistinguishably bound to AMP, ADSL-SAMP has its active sites 1 and 2 filled with AMP and fumarate, while the SAMP was observed in active sites 2 and 4 (Fig 14a,b). Both of these ligand bound structures previously have alluded to ADSL active sites being formed by three contributing monomers. For example, in the active site 1, the monophosphate group of AMP hydrogen bonds to three residues from chain A. The fumarate interacts with 3 residues from chain A bridging across to interactions with two residues from chain B, and one from chain D (Fig. 14a).

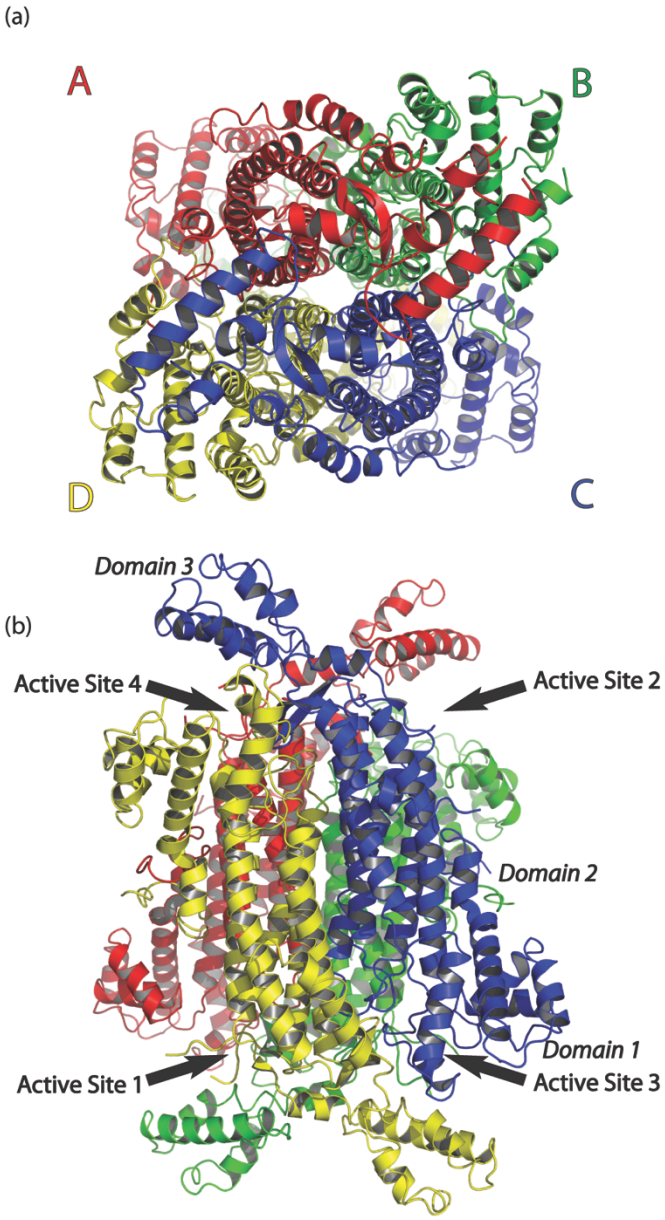

Figure 13: Side and Top view of WT homo-tetramer. $P2_12_12_1$ asymmetric unit of WT crystal. Monomers A, B, C and D are rendered red, green, blue, and yellow, respectively. Domains 1-3 are indicated for Monomer C. Active sites are indicated with arrows.

The ADSL-SAMP active sites with SAMP bound have similar intermonomeric interactions (Fig. 14b). Not surprisingly, upon inspection of the corresponding active site of R303C ADSL, density for the R303 side chain is largely absent with only enough remaining to represent a mutation to cysteine at that position (Fig. 14c). Based on the

ligand bound structures, this mutation would appear to simply eliminate the hydrogen bonds formed between the monophosphate in the AMP, or SAMP, and ADSL. This loss of the phosphate-R303 interaction, which also likely exists with AICAR, could be reflected in the enthalpy change detected by ITC for AMP and AICAR. However, upon closer examination by superimposing the active sites of R303C-ADSL with the corresponding sites in ADSL-SAMP revealed that the two structures' corresponding active sites are not entirely identical, giving possible credence to an earlier study's suggestion that the R303C mutation may disrupt the active site cleft (Zikánová et al. 2010). Specifically, comparison of R303C-ADSL's active sites with ADSL-SAMP's corresponding fumarate and AMP bound active sites shows a 2.5 Å shift of α-helices 2, 3 and 4 (Fig. 15a). This shift is also observed between R303-ADSL and ADSL-AMP. Interestingly similar, but not exact, shifts are also observed between R303C-ADSL's active sites and the SAMP filled active sites of ADSL-SAMP. To determine if the shift in α-helices 2 – 4 was related to the R303C mutation or a conformational change related to substrate binding, the structure of WT ADSL in its apo form (WT-ADSL-apo) was elucidated to 2.70 Å (Fig. 15b). Similar to the ADSL-R303C and ADSL-SAMP, electron density for residues 283–293 (β3-α10 loop) was not observed. Similarly to R303C-ADSL, WT-ADSL's monomers were largely indistinguishable outside of the domain 3. Intriguingly, comparison of the WT-ADSL-apo with ADSL-SAMP revealed a 2.7 Å shift of α-helices 2 – 4 in line to those observed previously in the R303C-ADSL and ADSL-SAMP comparison, indicating that substrate binding is likely the major cause of the shifts observed between the ADSL-R303C and the ADSL-SAMP (Fig. 15c), while comparison

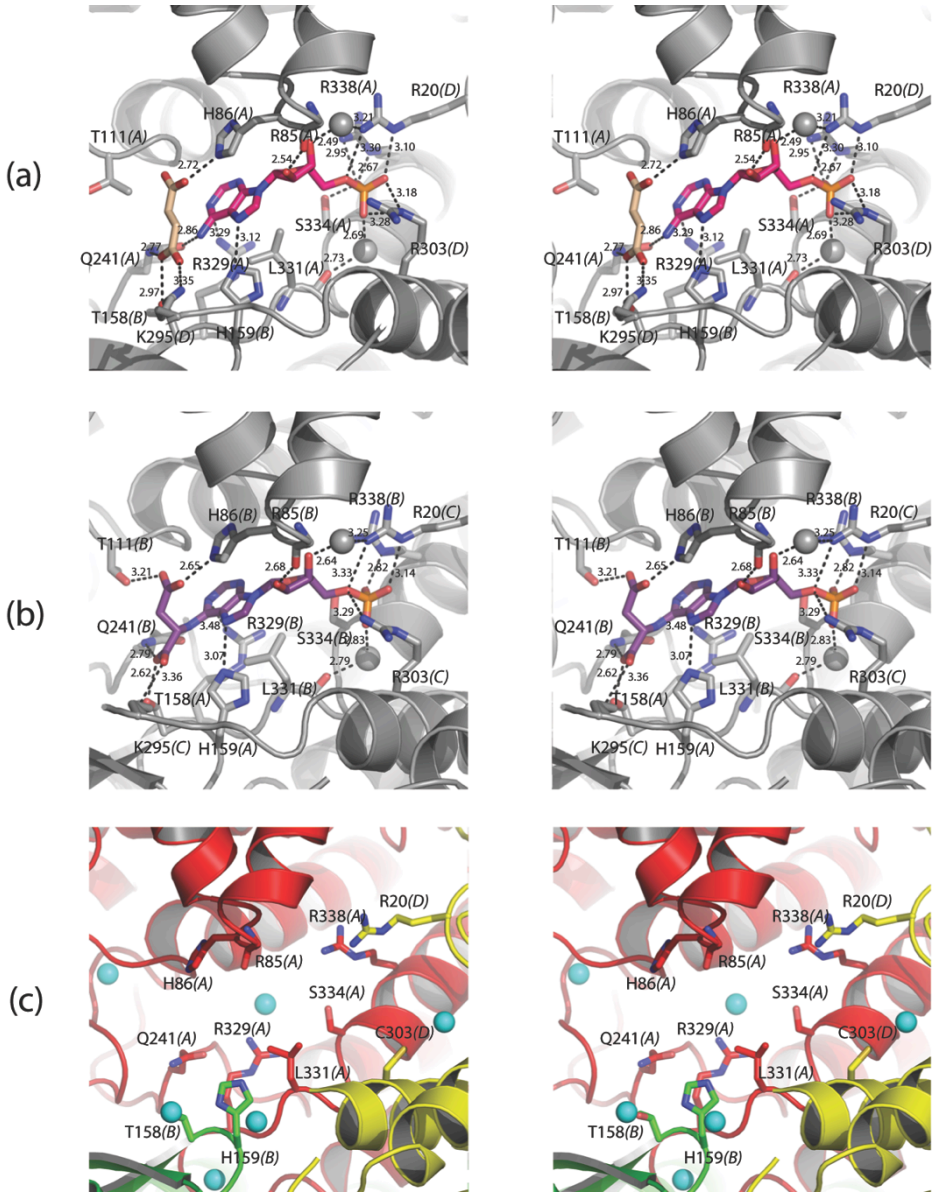

Figure 14: Comparison of ADSL active sites for WT, WT with substrate, and R303C mutant. (a) Wall-eyed stereo view of an ADSL-SAMP active site with AMP and fumarate occupying the active site. AMP is rendered pink and fumarate is rendered tan. Heteroatoms are colored according to their element. Water molecules (grey) are depicted as spheres and are scaled to 50% for clarity. The monomer each residue belongs to is given in parentheses after the residue number. (b) Wall-eyed stereo view of an ADSL-SAMP active site with SAMP occupying the active site. SAMP is rendered purple, and heteroatoms and water molecules are as in (a). (c) Wall-eyed stereo view of R303C ADSL active site. Monomers A, B and D are rendered red, green, and yellow, respectively. Heteroatoms are colored according to their element. Water molecules (cyan) are depicted as spheres and are scaled to 50%, and the side chain of R85 is hidden for clarity.

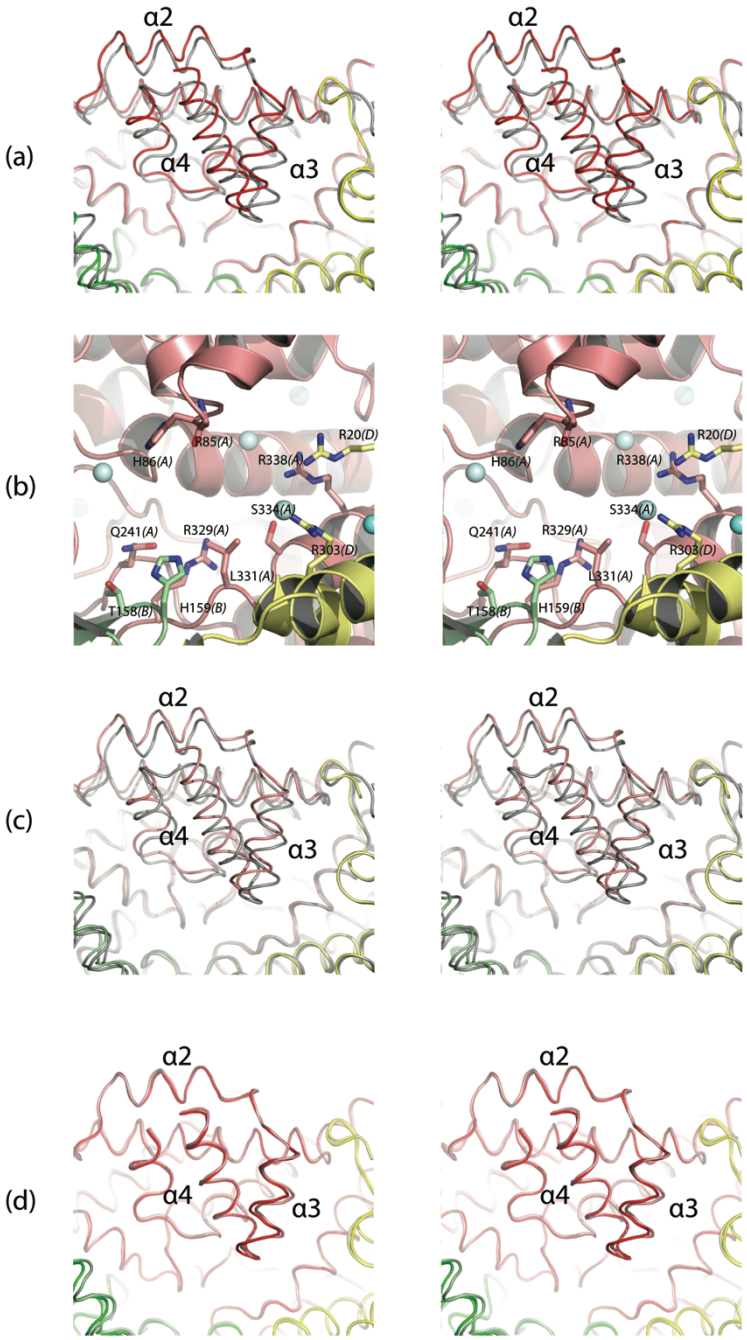

Figure 15: Substrate induced α-helices 2, 3 and 4 shift. (a) Wall eyed stereo view comparing the mobile loop α2-α4 between ADSL-SAMP (grey) and R303C-ADSL. (b) Wall-eyed stereo view of WT active site colored salmon, light yellow and pale green, with waters colored aqua. Heteroatoms are colored according to their element. Water molecules are depicted as spheres and are scaled to 50%, and the side chain of R85 is hidden for clarity. The monomer each residue belongs to is given in parentheses after the residue number. (c) Wall eyed stereo view comparing the mobile loop α2-α4 between ADSL-SAMP and WT ADSL. Coloring is as in (a) and (b). (d) Wall eyed stereo view comparing the mobile loop α2-α4 between R303C and WT ADSL. Coloring is as in (a) and (c).

of WTADSL-apo to R303C-ADSL revealed nearly identical structures (Fig. 15d). In addition, WTADSL-apo reveals an additional apo form of the ADSL active site that is divergent from product and substrate bound active sites previously observed.

Modeling of AMP/AICAR and Fumarate Binding in the Active Site

Currently, no crystal structure for WT ADSL with AICAR bound has been resolved. Utilizing the elucidated WT-ADSL-apo and ADSL-SAMP structures along with the understanding of local active site shifts within the active site upon substrate binding; AICAR and fumarate were modeled into the active site. Specifically, the AMP and fumarate bound active site of 2VD6 was employed as a template for the initial location of AICAR and fumarate within an active site of the WT-ADSL-apo. Using the Amber10 simulation package, by energy minimization the ADSL-AICAR-fumarate model structure was determined (Fig. 16a). To validate the modeling parameters used, we also energy minimized the structure with AMP and fumarate instead in the WT-ADSL-apo active site. The resulting AMP and fumarate bound ADSL model was nearly identical to that of AMP and fumarate bound in ADSL-SAMP.

As is evident from the figure, the placement of the fumarate, phosphate and ribose groups of AICAR and SAMP within the ADSL active site is similar (Fig. 16b). However, the remaining structure of the two substrates forms divergent interactions within the active site. This divergence could be a result of a rotatable bond between AICAR's imidazole ring and carbonyl carbon, whereas the presence of the pyrimidine in AMP eliminates the ability of the corresponding bond to rotate (Toth and Yeates 2000). As a result, this flexibility in AICAR and an amine group substituent of its imidazole ring

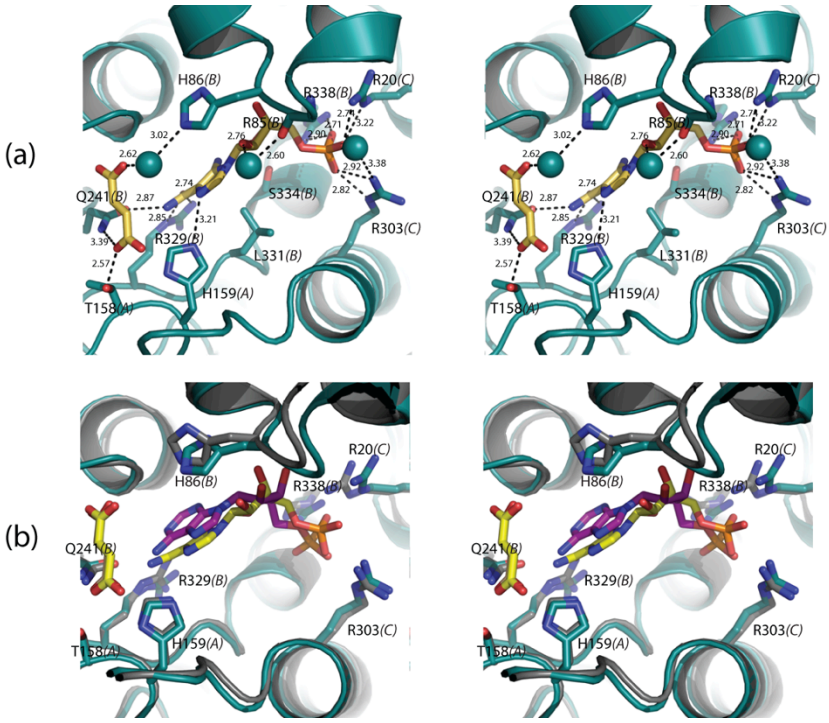

Figure 16: ADSL-AICAR-fumarate model. (a) Wall-eyed stereo view of model of WT active site with AICAR and fumarate occupying the active site. AICAR and fumarate are rendered yellow. Heteroatoms are colored according to their element. The monomer to which each residue belongs is given in parentheses after the residue number. (b) View of model of WT active site with AMP and fumarate overlaying model of WT active site with AICAR and fumarate. WT with AMP is rendered grey with AMP in pink and fumarate in tan, while WT with AICAR residues are teal with AICAR and fumarate in yellow.

potentially allows the amine to stick out in a space previously occupied by a water molecule potentially facilitating hydrogen bond with the hydroxyl group of the conserved S334 (Fig 12). Additionally, the rotation of the AICAR amide causes an alteration in the R329 side chain to form a hydrogen bond with AICAR's amide group.

Discussion

Origins of ADSL Cooperativity

The elucidation of the ADSL-SAMP structure has previously been suggested to support cooperativity in human ADSL, as AMP and fumarate are found in two active sites and with the other two occupied by SAMP. However, previously limited

biochemical data existed to support the origins or form of the cooperativity found in ADSL. Interestingly, the kinetic and thermodynamic properties of the WT ADSL and the R303C mutant suggest that the involvement of all three monomers that comprise an ADSL active site is necessary to achieve ADSL's positive cooperativity. Specifically, no cooperativity was observed when binding AICAR, or AMP, to WT ADSL. Binding of these products form the majority of their interactions with only two of the monomers. For example, in active site 1, AMP interacts with six residues from monomer A, and one from monomer B. Additionally, the phosphate group of AMP is anchored with two additional residues from a relatively immobile portion of monomer D. (Fig. 14a). This leaves the fumarate product to span interactions between monomer A's mobile α-helices 2 – 4, monomer B, and the near β3-α10 catalytic loop region of monomer D, suggesting that it is necessary for cooperativity to be observed. In line with this hypothesis, mutation of R303 to cysteine, which removes two hydrogen bonds, thus removing the majority of the interactions between monomer D and SAMP, results in no cooperativity (Fig. 14b).

Beyond the necessity for the substrate, or products, to involve all three monomers when binding to achieve an allosteric response, comparison of the WT-ADSL-apo and ADSL-SAMP active sites provided a glimpse into the model of allosteric regulation that ADSL undergoes. Specifically, the WT-ADSL-apo active sites are considerably more open to the bulk solvent then those of the ADSL-SAMP and ADSL-AMP structures (Fig. 17a). The 2.7 Å shift of α-helices 2, 3 and 4 observed between the WT-ADSL-apo active sites and those bound with AMP, or AMP and fumarate, illustrates a clamping down of the active site over SAMP, or AMP. With AICAR and SAICAR having homologous

phosphate, fumarate, and ribose moieties to that of AMP, the same shift is likely to occur upon the binding of these ligands as well. This closure of the active site around SAMP suggests that a concerted model of allosteric regulation would not be possible (Fig. 17c). In other words, if this shift occurred in a neighboring active site as a result of binding SAMP and SAICAR for the reaction running in the forward direction, SAMP attempting to bind to the neighboring active site would be sterically impeded. This would not be reflective of the positive cooperativity observed. Applying sequential allosteric regulation to the reverse reaction is less certain. The binding of AMP and AICAR would also be sterically impeded from binding to an active site that already underwent a shift of α-helices 2, 3 and 4. However, as illustrated by the thermodynamic information, the binding of AMP and AICAR is does not illustrate cooperativity. With fumarate binding at the top of the active site, which is exposed to the bulk solvent, a concerted model cannot be ruled out in the reverse direction (Fig. 16b).

Beyond the sequential model of allosteric modulation of ADSL, in what order, or the extent to which the active sites fill with substrates remains an open question. The ADSL-SAMP structure has its two active sites on the same end of ADSL occupied by SAMP and other distal active sites bound with fumarate and AMP. The absence of SAMP in all of the active sites could be due to restraints of the enzyme imposed by the crystal lattice, but alternatively might propose that substrates bind to adjacent active sites first, or only can bind to them. The latter would infer that the active sites at one end of the ADSL tetramer communicate to its distal neighbors. Although the mild loss of cooperativity observed by Ariyananda et al. (2009) by an ADSL mutation L311V at the

center of the tetramer would support this possibility, additional structurally guided mutagenesis along monomer interfaces and molecular dynamics simulations will be required to completely tease out the global allosteric nature of ADSL.

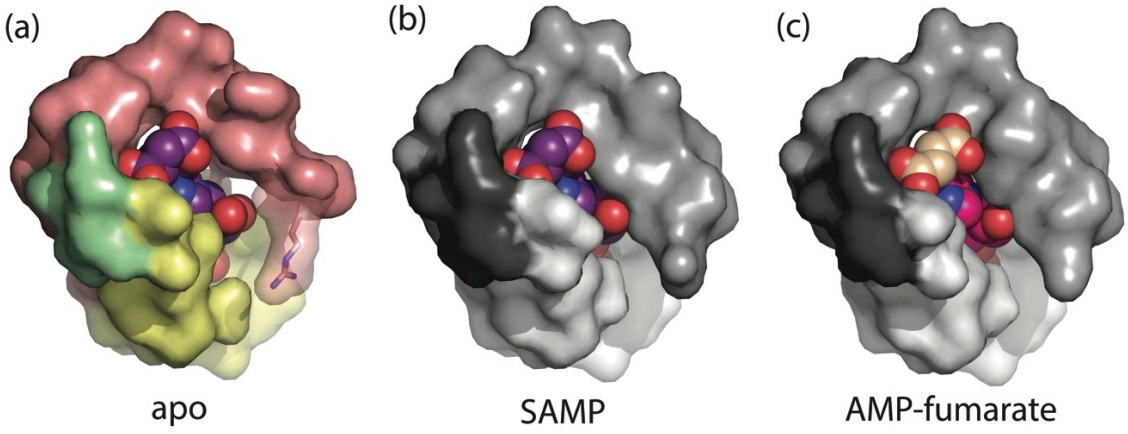

Figure 17: Constriction of the ADSL active site upon substrate binding. (a) Surface rendering of WT-ADSL-apo active site 1. WT active site depicted in salmon, light yellow and pale green corresponding to monomer A, B, and D respectively. R85 side chain is shown with transparency to reflect the lack of electron density for the side chain in all monomers. AMP and fumarate from active site 1 of ADSL-SAMP was placed in the apo active site for scaling purposes. (b) Surface rendering of SAMP and fumarate bound active site 1 of ADSL-SAMP. Coloring of light grey, medium grey, and dark grey correspond to monomers A, B, and D respectively. (c) Surface rendering of SAMP and fumarate bound active site of ADSL-SAMP. Coloring of light grey, medium grey, and dark grey correspond to monomers A, D, and C respectively. All waters were removed from surface renderings in (a-c).

Catalytic Effects of R303C Mutation

The loss of cooperativity because of the R303C mutation removal of hydrogen bonds with one of the three monomers comprising the active site as reflected in the structures of ADSL-SAMP, or ADSL-AMP, would not itself explain the divergent catalytic properties of ADSL observed towards SAICAR and SAMP. However, the combination of the kinetic and thermodynamic data coupled with the structural evidence suggests that the R303C mutation illuminates SAICAR as a better substrate for ADSL. At first glance, the unparallel reduction in k_{cat} between SAMP and SAICAR upon the R303C mutation could suggest that the divergence in catalytic ability of ADSL between SAMP

and SAICAR is due to a lack of substrate binding that favors SAICAR, or AICAR binding over that of SAMP. However, the K_M for SAICAR is slightly elevated relative to that of SAMP indicating that binding of SAICAR might be slightly weaker (Table 3). Moreover, the ADSL ligand bound structures have R303 forming hydrogen bonds to the phosphate group that is conserved between SAICAR and AICAR (Fig. 14). Also, the thermodynamic data reflects that the mutation causes a loss of enthalpy at almost equal magnitude for both AICAR and AMP, reflective of a loss of the same ADSL-phosphate group interactions. Despite the loss of the bond to the phosphate group, the overall ΔG_{bind} for both products remains similar to WT ADSL. This is accomplished by shifting the product binding from an unfavorable to favorable entropic event. The resulting K_d's for both substrates are nearly equally decreased by approximately 2.5–3 fold. This near equal drop in K_d but not k_{cat} suggests that the R303C mutation is indirectly affecting the catalytic ability of ADSL divergently for its two substrates. In other words, this thermodynamic, kinetic, and structural evidence suggests that the substrate can bind to the active site at a significant affinity despite the R303C mutation. As a result, unlike WT ADSL, the R303C mutant is likely operating at rapid equilibrium state, where if the substrate binds to ADSL, most substrate will dissociate, and only a small amount will be converted to product.

This would suggest that ADSL is more efficient at cleaving the fumarate-AICAR/AMP bond of SAICAR than SAMP. The inequality of catalysis might suggest that SAICAR and SAMP do not follow the same mechanistic pathway. The reaction mechanism for conversion of SAMP and SAICAR by ADSL has been previously

described as a general acid-base mechanism resulting in β-elimination of fumarate (Fig. 18) (Tsai et al. 2007). Although, the conversion of SAICAR to AICAR and fumarate could follow the same steps as the SAMP to AMP mechanism, due to the presence of an

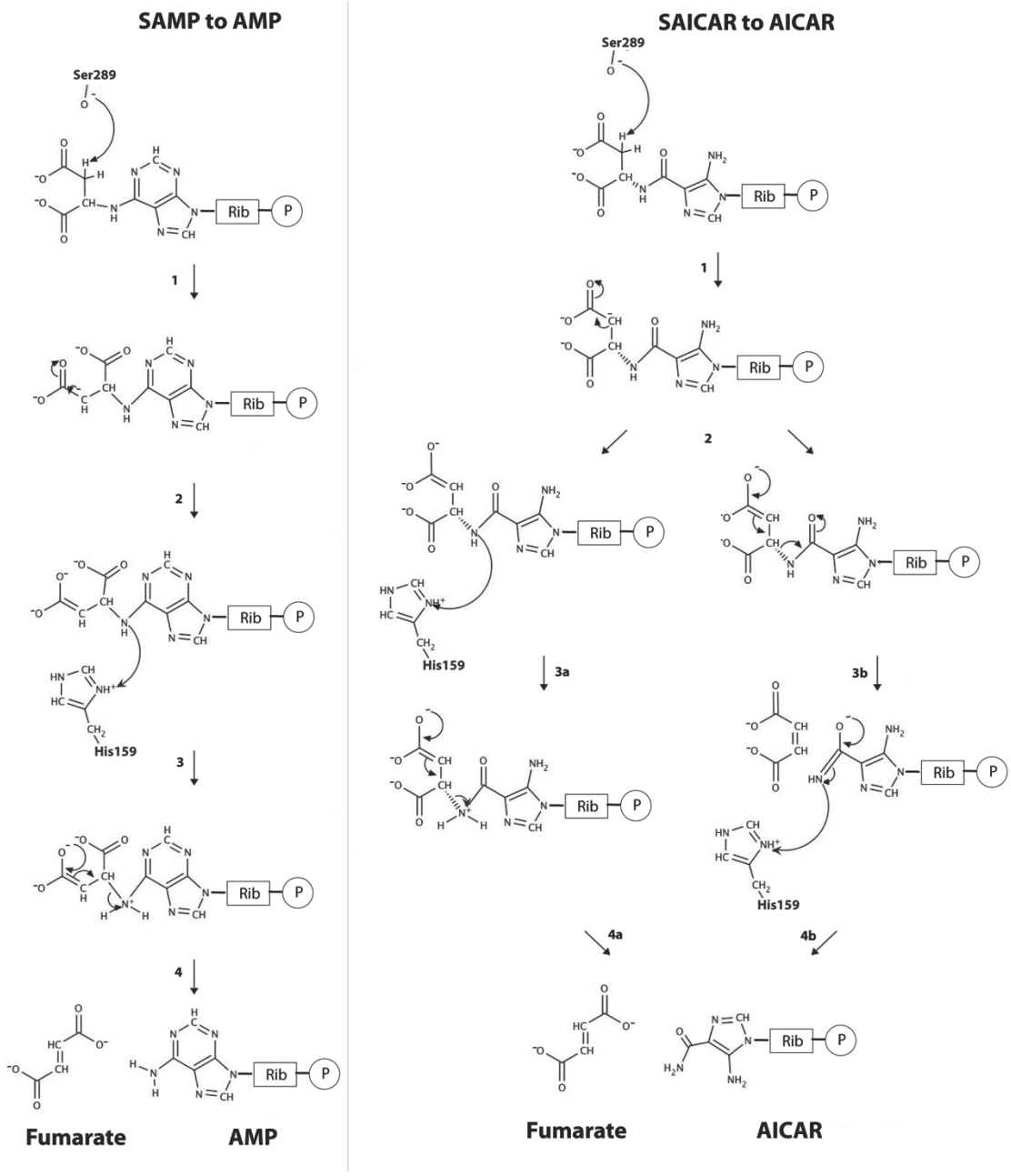

Figure 18: Proposed mechanism for SAICAR to AICAR plus fumarate and for SAMP to AMP plus fumarate.

additional carbonyl in SAICAR, there is another possibility. In this SAICAR selective pathway, the first two steps are the same: the C^{β}-proton is removed, and the negative charge is stabilized by the δ-carboxyl group. However, in the third step, as the electron density from the double-negatively charge carboxyl group is shifted down and the C^{α}-N6 bond is broken, a double bond is formed between N6 and the carbonyl carbon, and electron density is pushed up onto the carbonyl oxygen. Then, in the last step, this negative charge moves back down to form a C-O double bond as N6 becomes protonated by H159. This negatively charged oxygen may be stabilized by nearby positively charged residue, R235. This additional stabilization of the intermediate may be a factor in the faster reaction rate of SAICAR compared to SAMP.

An alternative possibility, or potential additional factor, for the inequality of bond cleavage between SAMP and SAICAR is the ability of SAICAR to be positioned with the active site in a more catalytically effective orientation than SAMP. The loss of the hydrogen bonds that R303 contributed to substrate binding potentially affected the ability to orient SAMP and SAICAR ideally for cleavage. Unlike SAMP, which possess a pyrimidine ring, SAICAR has a single rotatable bond that has been previously suggested to infer greater flexibility to adopt different conformations (Toth and Yeates 2000). This also might explain the lack of unparallel reduction in catalytic ability of *B. subtilis* ADSL. In that case, *B. subtilis* ADSL has an arginine in place of human ADSL T354 that may provide a similar influence. Unfortunately in the Palenchar and Colman (2003) study that looked at *B. subtilis* ADSL corresponding human ADSL R303C mutation (*B. subtilis* ADSL N276C), only performed a double mutation to mimic the human active site

configuration and did not include a single mutation for the corresponding arginine at human ADSL's T354. This prevented observing whether elimination of anchoring ADSL's substrates by a third arginine resulted in unparallel catalytic ability.

Additionally, the thermodynamic data suggests that AICAR forms an additional hydrogen bond not present in the ADSL-AMP complex. The enthalpic divergence between the two substrates remains after the introduction of the R303C mutation. The ability of SAICAR to possess an additional point of contact within the ADSL active site could ensure that SAICAR properly oriented within the active site more often then SAMP, contributing to the unparallel k_{cat} between SAMP and SAICAR observed. Based on the ADSL-AICAR-fumarate model, the additional hydrogen bond could be reflective of an interaction between AICAR and the highly conserved S334 (Fig 16a). Curiously, even in human ADSL's distant homolog of *B. subtilis*, this serine is conserved. This serine has not previously been implicated in substrate binding or catalysis, as it does not interact directly with SAMP or AMP within the ADSL-SAMP and ADSL-AMP structures. Naturally, additional site-directed mutagenesis efforts within the active site including S334, or an X-ray structure of ADSL with SAICAR, or AICAR, will be necessary to fully identify the ADSL residue acceptor that forms the additional hydrogen bond with AICAR and bring final clarity to the unparallel catalytic activity observed.

REFERENCES

Adams, Paul D., Pavel V. Afonine, Gabor Bunkoczi, Vincent B. Chen, Ian W. Davis, Nathaniel Echols, Jeffrey J. Headd, Li-Wei Hung, Gary J. Kapral, Ralf W. Grosse-Kunstleve, Airlie J. McCoy, Nigel W. Moriarty, Robert Oeffner, Randy J. Read, David C. Richardson, Jane S. Richardson, Thomas C. Terwilliger, and Peter H. Zwart. 2010. "PHENIX: a comprehensive Python-based system for macromolecular structure solution." *Acta Crystallographica Section D* no. 66 (2):213-221. doi: doi:10.1107/S0907444909052925.

Akutsu, M., Y. Ye, S. Virdee, J. W. Chin, and D. Komander. 2011. "Molecular basis for ubiquitin and ISG15 cross-reactivity in viral ovarian tumor domains." *Proc Natl Acad Sci U S A* no. 108 (6):2228-33. doi: 10.1073/pnas.1015287108.

Alkalay, I., A. Yaron, A. Hatzubai, A. Orian, A. Ciechanover, and Y. Ben-Neriah. 1995. "Stimulation-dependent I kappa B alpha phosphorylation marks the NF-kappa B inhibitor for degradation via the ubiquitin-proteasome pathway." *Proc Natl Acad Sci U S A* no. 92 (23):10599-603.

An, T. Q., Z. J. Tian, Y. J. Zhou, Y. Xiao, J. M. Peng, J. Chen, Y. F. Jiang, X. F. Hao, and G. Z. Tong. 2011. "Comparative genomic analysis of five pairs of virulent parental/attenuated vaccine strains of PRRSV." *Veterinary Microbiology* no. 149 (1-2):104-12. doi: 10.1016/j.vetmic.2010.11.001.

Ariyananda, Lushanti De Zoysa, Christina Antonopoulos, Jenna Currier, and Roberta F. Colman. 2011. "In Vitro Hybridization and Separation of Hybrids of Human Adenylosuccinate Lyase from Wild-Type and Disease-Associated Mutant Enzymes." *Biochemistry* no. 50 (8):1336-1346. doi: Doi 10.1021/Bi101734q.

Ariyananda, Lushanti De Zoysa, Peychii Lee, Christina Antonopoulos, and Roberta F. Colman. 2009. "Biochemical and Biophysical Analysis of Five Disease-Associated Human Adenylosuccinate Lyase Mutants." *Biochemistry* no. 48 (23):5291-5302. doi: Doi 10.1021/Bi802321m.

Baresova, Veronika, Vaclava Skopova, Jakub Sikora, David Patterson, Jana Sovova, Marie Zikanova, and Stanislav Kmoch. 2012. "Mutations of ATIC and ADSL affect purinosome assembly in cultured skin fibroblasts from patients with AICA-ribosiduria and ADSL deficiency." *Human Molecular Genetics* no. 21 (7):1534-1543.

Brockmeier, S. L., C. L. Loving, A. C. Vorwald, M. E. Kehrli, Jr., R. B. Baker, T. L. Nicholson, K. M. Lager, L. C. Miller, and K. S. Faaberg. 2012. "Genomic sequence and virulence comparison of four Type 2 porcine reproductive and

respiratory syndrome virus strains." *Virus Research* no. 169 (1):212-21. doi: 10.1016/j.virusres.2012.07.030.

Brosius, Jennifer L., and Roberta F. Colman. 2002. "Three subunits contribute amino acids to the active site of tetrameric adenylosuccinate lyase: Lys(268) and Glu(275) are required." *Biochemistry* no. 41 (7):2217-2226. doi: Doi 10.1021/Bi011998t.

Capodagli, G. C., M. A. McKercher, E. A. Baker, E. M. Masters, J. S. Brunzelle, and S. D. Pegan. 2011. "Structural analysis of a viral ovarian tumor domain protease from the Crimean-Congo hemorrhagic fever virus in complex with covalently bonded ubiquitin." *Journal of Virology* no. 85 (7):3621-30. doi: JVI.02496-10 [pii] 10.1128/JVI.02496-10.

Capodagli, Glenn C., Michelle K. Deaton, Erica A. Baker, Ryan J. Lumpkin, and Scott D. Pegan. 2013. "Diversity of Ubiquitin and ISG15 Specificity among Nairoviruses' Viral Ovarian Tumor Domain Proteases." *Journal of Virology* no. 87 (7):3815-3827.

Case, D. A., T. E. Cheatham, T. Darden, H. Gohlke, R. Luo, K. M. Merz, A. Onufriev, C. Simmerling, B. Wang, and R. J. Woods. 2005. "The Amber biomolecular simulation programs." *Journal of Computational Chemistry* no. 26 (16):1668-1688. doi: Doi 10.1002/Jcc.20290.

Chand, Ranjni J., Benjamin R. Trible, and Raymond R. R. Rowland. 2012. "Pathogenesis of porcine reproductive and respiratory syndrome virus." *Current Opinion in Virology* no. 2 (3):256-263. doi: http://dx.doi.org/10.1016/j.coviro.2012.02.002.

Chen, Z., J. Hagler, V. J. Palombella, F. Melandri, D. Scherer, D. Ballard, and T. Maniatis. 1995. "Signal-induced site-specific phosphorylation targets I kappa B alpha to the ubiquitin-proteasome pathway." *Genes Dev* no. 9 (13):1586-97.

Ciardo, Francesca, Costantino Salerno, and Paolo Curatolo. 2001. "Neurologic aspects of adenylosuccinate lyase deficiency." *Journal of Child Neurology* no. 16 (5):301-308.

den Boon, J. A., K. S. Faaberg, J. J. Meulenberg, A. L. Wassenaar, P. G. Plagemann, A. E. Gorbalenya, and E. J. Snijder. 1995. "Processing and evolution of the N-terminal region of the arterivirus replicase ORF1a protein: identification of two papainlike cysteine proteases." *J Virol* no. 69 (7):4500-5.

Dilcher, Meik, Andrea Koch, Lekbira Hasib, Gerhard Dobler, Frank Hufert, and Manfred Weidmann. 2012. "Genetic characterization of Erve virus, a European Nairovirus

distantly related to Crimean-Congo hemorrhagic fever virus." *Virus Genes*:1-7. doi: 10.1007/s11262-012-0796-8.

Ellingson, J. S., Y. Wang, S. Layton, J. Ciacci-Zanella, M. B. Roof, and K. S. Faaberg. 2010. "Vaccine efficacy of porcine reproductive and respiratory syndrome virus chimeras." *Vaccine* no. 28 (14):2679-86. doi: S0264-410X(10)00009-5 [pii] 10.1016/j.vaccine.2009.12.073.

Emsley, P., and K. Cowtan. 2004. "Coot: model-building tools for molecular graphics." *Acta Crystallogr D Biol Crystallogr* no. 60 (Pt 12 Pt 1):2126-32. doi: S0907444904019158 [pii] 10.1107/S0907444904019158.

Frias-Staheli, N., N. V. Giannakopoulos, M. Kikkert, S. L. Taylor, A. Bridgen, J. Paragas, J. A. Richt, R. R. Rowland, C. S. Schmaljohn, D. J. Lenschow, E. J. Snijder, A. Garcia-Sastre, and H. W. 4th Virgin. 2007. "Ovarian tumor domain-containing viral proteases evade ubiquitin- and ISG15-dependent innate immune responses." *Cell Host Microbe* no. 2 (6):404-16. doi: S1931-3128(07)00249-1 [pii] 10.1016/j.chom.2007.09.014.

Georges, JaakJaeken, and VanDen Berghe. 1984. "An Infantile Autistic Syndrome Characterized by the Presence of Succinyl Purines in Body-Fluids." *Lancet* no. 2 (8411):1058-1061.

Gill, S. C., and P. H. von Hippel. 1989. "Calculation of protein extinction coefficients from amino acid sequence data." *Anal Biochem* no. 182 (2):319-26.

Gitiaux, Cyril, Irène Ceballos-Picot, Sandrine Marie, Vassili Valayannopoulos, Marlène Rio, Séverine Verrieres, Jean François Benoist, Marie Françoise Vincent, Isabelle Desguerre, and Nadia Bahi-Buisson. 2009. "Misleading behavioural phenotype with adenylosuccinate lyase deficiency." *European Journal of Human Genetics* no. 17 (1):133-136. doi: Doi 10.1038/Ejhg.2008.174.

Guo, B., K. M. Lager, J. N. Henningson, L. C. Miller, S. N. Schlink, M. A. Kappes, M. E. Kehrli, Jr., S. L. Brockmeier, T. L. Nicholson, H. C. Yang, and K. S. Faaberg. 2013. "Experimental infection of United States swine with a Chinese highly pathogenic strain of porcine reproductive and respiratory syndrome virus." *Virology* no. 435 (2):372-84. doi: 10.1016/j.virol.2012.09.013.

Guo, Baoqing, Kelly M. Lager, Sarah N. Schlink, Marcus E. Kehrli Jr, Susan L. Brockmeier, Laura C. Miller, Sabrina L. Swenson, and Kay S. Faaberg. 2013. "Chinese and Vietnamese strains of HP-PRRSV cause different pathogenic outcomes in United States high health swine." *Virology* no. 446 (1–2):238-250. doi: http://dx.doi.org/10.1016/j.virol.2013.08.008.

Han, J., M. S. Rutherford, and K. S. Faaberg. 2009. "The porcine reproductive and respiratory syndrome virus nsp2 cysteine protease domain possesses both trans- and cis-cleavage activities." *Journal of Virology* no. 83 (18):9449-63. doi: JVI.00834-09 [pii] 10.1128/JVI.00834-09.

Han, J., Y. Wang, and K. S. Faaberg. 2006. "Complete genome analysis of RFLP 184 isolates of porcine reproductive and respiratory syndrome virus." *Virus Res* no. 122 (1-2):175-82. doi: S0168-1702(06)00189-4 [pii] 10.1016/j.virusres.2006.06.003.

Han, M., Y. Du, C. Song, and D. Yoo. 2013. "Degradation of CREB-binding protein and modulation of type I interferon induction by the zinc finger motif of the porcine reproductive and respiratory syndrome virus nsp1alpha subunit." *Virus Res* no. 172 (1-2):54-65. doi: 10.1016/j.virusres.2012.12.012.

Han, W., J. J. Wu, X. Y. Deng, Z. Cao, X. L. Yu, C. B. Wang, T. Z. Zhao, N. H. Chen, H. H. Hu, W. Bin, L. L. Hou, L. L. Wang, K. G. Tian, and Z. Q. Zhang. 2009. "Molecular mutations associated with the in vitro passage of virulent porcine reproductive and respiratory syndrome virus." *Virus Genes* no. 38 (2):276-84. doi: 10.1007/s11262-008-0322-1.

Hornak, V., R. Abel, A. Okur, B. Strockbine, A. Roitberg, and C. Simmerling. 2006. "Comparison of multiple amber force fields and development of improved protein backbone parameters." *Proteins-Structure Function and Bioinformatics* no. 65 (3):712-725. doi: Doi 10.1002/Prot.21123.

Huang, J., S. Zhao, M. Zhu, Z. Wu, and M. Yu. 2009. "Sequence and expression analyses of porcine ISG15 and ISG43 genes." *Comp Biochem Physiol B Biochem Mol Biol* no. 153 (4):301-9. doi: 10.1016/j.cbpb.2009.03.006.

Hürlimann, Hans C., Benoît Laloo, Barbara Simon-Kayser, Christelle Saint-Marc, Fanny Coulpier, Sophie Lemoine, Bertrand Daignan-Fornier, and Benoît Pinson. 2011. "Physiological and Toxic Effects of Purine Intermediate 5-Amino-4-imidazolecarboxamide Ribonucleotide (AICAR) in Yeast." *The Journal of Biological Chemistry* no. 286 (35):30994-31002. doi: 10.1074/jbc.M111.262659.

Ishii, A., K. Ueno, Y. Orba, M. Sasaki, L. Moonga, B. M. Hang'ombe, A. S. Mweene, T. Umemura, K. Ito, W. W. Hall, and H. Sawa. 2014. "A nairovirus isolated from African bats causes haemorrhagic gastroenteritis and severe hepatic disease in mice." *Nat Commun* no. 5:5651. doi: 10.1038/ncomms6651.

James, Terrence W., Natalia Frias-Staheli, John-Paul Bacik, Jesica M. Levingston Macleod, Mazdak Khajehpour, Adolfo García-Sastre, and Brian L. Mark. 2011. "Structural basis for the removal of ubiquitin and interferon-stimulated gene 15 by

a viral ovarian tumor domain-containing protease." *Proceedings of the National Academy of Sciences* no. 108 (6):2222-2227. doi: 10.1073/pnas.1013388108.

Jiang, X., L. N. Kinch, C. A. Brautigam, X. Chen, F. Du, N. V. Grishin, and Z. J. Chen. 2012. "Ubiquitin-induced oligomerization of the RNA sensors RIG-I and MDA5 activates antiviral innate immune response." *Immunity* no. 36 (6):959-73. doi: 10.1016/j.immuni.2012.03.022.

Jorgensen, W. L., J. Chandrasekhar, J. D. Madura, R. W. Impey, and M. L. Klein. 1983. "Comparison of Simple Potential Functions for Simulating Liquid Water." *Journal of Chemical Physics* no. 79 (2):926-935.

Jurecka, Agnieszka, Marie Zikanova, Anna Tylki-Szymanska, Jakub Krijt, Anna Bogdanska, Wanda Gradowska, Karolina Mullerova, Jolanta Sykut-Cegielska, Stanislav Kmoch, and Ewa Pronicka. 2008. "Clinical, biochemical and molecular findings in seven Polish patients with adenylosuccinate lyase deficiency." *Molecular Genetics and Metabolism* no. 94 (4):435-442. doi: Doi 10.1016/J.Ymgme.2008.04.013.

Kim, K. I., and D. E. Zhang. 2005. "UBP43, an ISG15-specific deconjugating enzyme: expression, purification, and enzymatic assays." *Methods Enzymol* no. 398:491-9. doi: 10.1016/S0076-6879(05)98040-3.

Kim, O., Y. Sun, F. W. Lai, C. Song, and D. Yoo. 2010. "Modulation of type I interferon induction by porcine reproductive and respiratory syndrome virus and degradation of CREB-binding protein by non-structural protein 1 in MARC-145 and HeLa cells." *Virology* no. 402 (2):315-26. doi: 10.1016/j.virol.2010.03.039.

Kmoch, Stanislav, Hana Hartmannová, Blanka Stibùrková, Jakub Krijt, Marie Zikánová, and Ivan Šebesta. 2000. "Human adenylosuccinate lyase (ADSL), cloning and characterization of full-length cDNA and its isoform, gene structure and molecular basis for ADSL deficiency in six patients." *Human Molecular Genetics* no. 9 (10):1501-1513.

Köhler, Martin, Birgit Assmann, Christa Bräutigam, Wolfgang Storm, Sandrine Marie, M. Françoise Vincent, Georges Van den Berghe, Anne H. Simmonds, and Georg F. Hoffmann. 1999. "Adenylosuccinase deficiency: possibly underdiagnosed encephalopathy with variable clinical features." *European Journal of Paediatric Neurology* no. 3 (1):3-6. doi: http://dx.doi.org/10.1053/ejpn.1999.0172.

Komander, D., M. J. Clague, and S. Urbe. 2009. "Breaking the chains: structure and function of the deubiquitinases." *Nature reviews. Molecular cell biology* no. 10 (8):550-63. doi: 10.1038/nrm2731.

Kulathu, Y., and D. Komander. 2012. "Atypical ubiquitylation - the unexplored world of polyubiquitin beyond Lys48 and Lys63 linkages." *Nat Rev Mol Cell Biol* no. 13 (8):508-23. doi: 10.1038/nrm3394.

Kwon, B., I. H. Ansari, A. K. Pattnaik, and F. A. Osorio. 2008. "Identification of virulence determinants of porcine reproductive and respiratory syndrome virus through construction of chimeric clones." *Virology* no. 380 (2):371-8. doi: S0042-6822(08)00490-X [pii] 10.1016/j.virol.2008.07.030.

Lee, P., and R. F. Colman. 2007. "Expression, purification, and characterization of stable, recombinant human adenylosuccinate lyase." *Protein Expression and Purification* no. 51 (2):227-234. doi: Doi 10.1016/J.Pep.2006.07.023.

Li, H., Z. Zheng, P. Zhou, B. Zhang, Z. Shi, Q. Hu, and H. Wang. 2010. "The cysteine protease domain of porcine reproductive and respiratory syndrome virus non-structural protein 2 antagonizes interferon regulatory factor 3 activation." *The Journal of general virology* no. 91 (Pt 12):2947-58. doi: 10.1099/vir.0.025205-0.

Li, Y., X. Wang, K. Bo, B. Tang, B. Yang, W. Jiang, and P. Jiang. 2007. "Emergence of a highly pathogenic porcine reproductive and respiratory syndrome virus in the Mid-Eastern region of China." *Vet J* no. 174 (3):577-84. doi: S1090-0233(07)00267-5 [pii] 10.1016/j.tvjl.2007.07.032.

Lundy, Claire T., Heinz Jungbluth, Keith R. E. Pohl, Ata Siddiqui, Anthony M. Marinaki, Helen Mundy, and Michael P. Champion. 2010. "Adenylosuccinate Lyase Deficiency in the United Kingdom Pediatric Population: First Three Cases." *Pediatric Neurology* no. 43 (5):351-354. doi: Doi 10.1016/J.Pediatrneurol.2010.06.007.

McCoy, A. J., R. W. Grosse-Kunstleve, P. D. Adams, M. D. Winn, L. C. Storoni, and R. J. Read. 2007. "Phaser crystallographic software." *J Appl Crystallogr* no. 40 (Pt 4):658-674. doi: 10.1107/S0021889807021206.

Messick, T. E., N. S. Russell, A. J. Iwata, K. L. Sarachan, R. Shiekhattar, J. R. Shanks, F. E. Reyes-Turcu, K. D. Wilkinson, and R. Marmorstein. 2008. "Structural basis for ubiquitin recognition by the Otu1 ovarian tumor domain protein." *J Biol Chem* no. 283 (16):11038-49. doi: M704398200 [pii] 10.1074/jbc.M704398200.

Mielech, Anna M., Yafang Chen, Andrew D. Mesecar, and Susan C. Baker. "Nidovirus papain-like proteases: Multifunctional enzymes with protease, deubiquitinating and deISGylating activities." *Virus Research* (0). doi: http://dx.doi.org/10.1016/j.virusres.2014.01.025.

Mouchegh, Katharina, Marie Zikánová, Georg F. Hoffmann, Benno Kretzschmar, Thomas Kühn, Eva Mildenberger, Gisela Stoltenburg-Didinger, Jakub Krijt, Lenka Dvořáková, Tomáš Honzík, Jiri Zeman, Stanislav Kmoch, and Rainer Rossi. 2007. "Lethal fetal and early neonatal presentation of adenylosuccinate lyase deficiency: Observation of 6 patients in 4 families." *Journal of Pediatrics* no. 150 (1):57-61. doi: Doi 10.1016/J.Jpeds.2006.09.027.

Murshudov, G. N., A. A. Vagin, and E. J. Dodson. 1997. "Refinement of macromolecular structures by the maximum-likelihood method." *Acta Crystallographica Section D-Biological Crystallography* no. 53:240-255.

Ni, Y. Y., T. Opriessnig, L. Zhou, D. Cao, Y. W. Huang, P. G. Halbur, and X. J. Meng. 2013. "Attenuation of porcine reproductive and respiratory syndrome virus by molecular breeding of virus envelope genes from genetically divergent strains." *J Virol* no. 87 (1):304-13. doi: 10.1128/JVI.01789-12.

Nielsen, H. S., M. B. Oleksiewicz, R. Forsberg, T. Stadejek, A. Botner, and T. Storgaard. 2001. "Reversion of a live porcine reproductive and respiratory syndrome virus vaccine investigated by parallel mutations." *J Gen Virol* no. 82 (Pt 6):1263-72.

Oshiumi, H., M. Miyashita, M. Matsumoto, and T. Seya. 2013. "A Distinct Role of Riplet-Mediated K63-Linked Polyubiquitination of the RIG-I Repressor Domain in Human Antiviral Innate Immune Responses." *PLoS Pathog* no. 9 (8):e1003533. doi: 10.1371/journal.ppat.1003533.

Otwinowski, Z., and W. Minor. 1997. "Processing of X-ray diffraction data collected in oscillation mode." *Macromolecular Crystallography, Pt A* no. 276:307-326.

Palenchar, Jennifer Brosius, and Roberta F. Colman. 2003. "Characterization of a mutant Bacillus subtilis adenylosuccinate lyase equivalent to a mutant enzyme found in human adenylosuccinate lyase deficiency: Asparagine 276 plays an important structural role." *Biochemistry* no. 42 (7):1831-1841. doi: Doi 10.1021/Bi020640+.

Pearlman, D. A., D. A. Case, J. W. Caldwell, W. S. Ross, T. E. Cheatham, S. Debolt, D. Ferguson, G. Seibel, and P. Kollman. 1995. "Amber, a package of computer-programs for applying molecular mechanics, normal-mode analysis, molecular-dynamics and free-energy calculations to simulate the structural and energetic properties of molecules." *Computer Physics Communications* no. 91 (1-3):1-41.

Race, Valérie, Sandrine Marie, Marie-Françoise Vincent, and Georges Van den Berghe. 2000. "Clinical, biochemical and molecular genetic correlations in adenylosuccinate lyase deficiency." *Human Molecular Genetics* no. 9 (14):2159-2165.

Ratia, Kiira, Andrew Kilianski, Yahira M. Baez-Santos, Susan C. Baker, and Andrew Mesecar. 2014. "Structural basis for the ubiquitin-linkage specificity and deISGylating activity of SARS-CoV papain-like protease." *PLoS Pathog* no. 10 (5):e1004113. doi: 10.1371/journal.ppat.1004113.

Shi, M., T. T. Lam, C. C. Hon, R. K. Hui, K. S. Faaberg, T. Wennblom, M. P. Murtaugh, T. Stadejek, and F. C. Leung. 2010. "Molecular epidemiology of PRRSV: a phylogenetic perspective." *Virus Research* no. 154 (1-2):7-17. doi: S0168-1702(10)00291-1 [pii] 10.1016/j.virusres.2010.08.014.

Shi, Y., Z. Hu, Z. Xiong, Y. Zhou, X. Jin, C. Gu, X. Hu, G. Cheng, N. Song, and W. Zhang. 2013. "Analysis of molecular variation of porcine reproductive and respiratory syndrome virus in Central China from 2006 to 2012." *Arch Virol* no. 158 (3):717-21. doi: 10.1007/s00705-012-1542-1.

Sivendran, Sharmila, and Roberta F. Colman. 2008. "Effect of a new non-cleavable substrate analog on wild-type and serine mutants in the signature sequence of adenylosuccinate lyase of Bacillus subtilis and Homo sapiens." *Protein Science* no. 17 (7):1162-1174. doi: Doi 10.1110/Ps.034777.108.

Sivendran, Sharmila, David Patterson, Erin Spiegel, Ivan McGown, David Cowley, and Roberta F. Colman. 2004. "Two novel mutant human adenylosuccinate Lyases (ASLs) associated with autism and characterization of the equivalent mutant Bacillus subtilis ASL." *Journal of Biological Chemistry* no. 279 (51):53789-53797. doi: Doi 10.1074/Jbc.M409974200.

Snijder, E. J., A. L. Wassenaar, W. J. Spaan, and A. E. Gorbalenya. 1995. "The arterivirus Nsp2 protease. An unusual cysteine protease with primary structure similarities to both papain-like and chymotrypsin-like proteases." *J Biol Chem* no. 270 (28):16671-6.

Song, C., P. Krell, and D. Yoo. 2010. "Nonstructural protein 1alpha subunit-based inhibition of NF-kappaB activation and suppression of interferon-beta production by porcine reproductive and respiratory syndrome virus." *Virology* no. 407 (2):268-80. doi: 10.1016/j.virol.2010.08.025.

Sorensen, Christina M., Lea A. Rempel, Shane R. Nelson, Brian R. Francis, David J. Perry, Randolph V. Lewis, Arthur L. Haas, and Thomas R. Hansen. 2007. "The Hinge Region between Two Ubiquitin-like Domains Destabilizes Recombinant ISG15 in Solution†." *Biochemistry* no. 46 (3):772-780. doi: 10.1021/bi061408x.

Spiegel, Erin K., Roberta F. Colman, and David Patterson. 2006. "Adenylosuccinate lyase deficiency." *Molecular Genetics and Metabolism* no. 89 (1-2):19-31. doi: Doi 10.1016/J.Ymgme.2006.04.018.

Stone, Randy L., Howard Zalkin, and Jack E. Dixon. 1993. "Expression, purification, and kinetic characterization of recombinant human adenylosuccinate lyase." *Journal of Biological Chemistry* no. 268 (26):19710-19716.

Storgaard, T., M. Oleksiewicz, and A. Botner. 1999. "Examination of the selective pressures on a live PRRS vaccine virus." *Arch Virol* no. 144 (12):2389-401. doi: 91442389.705 [pii].

Sun, Z., Z. Chen, S. R. Lawson, and Y. Fang. 2010. "The cysteine protease domain of porcine reproductive and respiratory syndrome virus nonstructural protein 2 possesses deubiquitinating and interferon antagonism functions." *Journal of Virology* no. 84 (15):7832-46. doi: 10.1128/JVI.00217-10.

Sun, Z., Y. Li, R. Ransburgh, E. J. Snijder, and Y. Fang. 2012. "Nonstructural protein 2 of porcine reproductive and respiratory syndrome virus inhibits the antiviral function of interferon-stimulated gene 15." *J Virol* no. 86 (7):3839-50. doi: 10.1128/JVI.06466-11.

Tokunaga, F., S. Sakata, Y. Saeki, Y. Satomi, T. Kirisako, K. Kamei, T. Nakagawa, M. Kato, S. Murata, S. Yamaoka, M. Yamamoto, S. Akira, T. Takao, K. Tanaka, and K. Iwai. 2009. "Involvement of linear polyubiquitylation of NEMO in NF-kappaB activation." *Nat Cell Biol* no. 11 (2):123-32. doi: 10.1038/ncb1821.

Toth, Eric A., Carolyn Worby, Jack E. Dixon, Eric R. Goedken, Susan Marqusee, and Todd O. Yeates. 2000. "The crystal structure of adenylosuccinate lyase from Pyrobaculum aerophilum reveals an intracellular protein with three disulfide bonds." *Journal of Molecular Biology* no. 301 (2):433-450.

Toth, Eric A., and Todd O. Yeates. 2000. "The structure of adenylosuccinate lyase, an enzyme with dual activity in the de novo purine biosynthetic pathway." *Structure with Folding & Design* no. 8 (2):163-174.

Tsai, May, Jason Koo, Patrick Yip, Roberta F. Colman, Mark L. Segal, and P. Lynne Howell. 2007. "Substrate and product complexes of Escherichia coli adenylosuccinate lyase provide new insights into the enzymatic mechanism." *Journal of Molecular Biology* no. 370 (3):541-554. doi: Doi 10.1016/J.Jmb.2007.04.052.

Van den Bergh, F., Marie-Françoise Vincent, Jacques Jaeken, and Georges Van den Berghe. 1993. "Residual adenylosuccinase activities in fibroblasts of adenylosuccinase-deficient children: parallel deficiency with adenylosuccinate and succinyl-AICAR in profoundly retarded patients and non-parallel deficiency

in a mildly retarded girl." *Journal of Inherited Metabolic Disease* no. 16 (2):415-424.

Van den Bergh, F., Marie-Françoise Vincent, Jacques Jaeken, and Georges Van den Berghe. 1993. "Functional studies in fibroblasts of adenylosuccinase-deficient children." *Journal of inherited metabolic disease* no. 16 (2):425-434.

van Hemert, M. J., and E. J. Snijder. 2008. "The Arterivirus Replicase." In *The Nidoviruses*, edited by Thomas Gallaher and Eric Snjder Stanley Perlman, 83-101. Washington, DC: ASM Press.

van Kasteren, P. B., C. Beugeling, D. K. Ninaber, N. Frias-Staheli, S. van Boheemen, A. Garcia-Sastre, E. J. Snijder, and M. Kikkert. 2012. "Arterivirus and nairovirus ovarian tumor domain-containing Deubiquitinases target activated RIG-I to control innate immune signaling." *Journal of Virology* no. 86 (2):773-85. doi: 10.1128/JVI.06277-11.

Wang, Y., Y. Liang, J. Han, K. M. Burkhart, E. M. Vaughn, M. B. Roof, and K. S. Faaberg. 2008. "Attenuation of porcine reproductive and respiratory syndrome virus strain MN184 using chimeric construction with vaccine sequence." *Virology* no. 371 (2):418-29. doi: S0042-6822(07)00628-9 [pii] 10.1016/j.virol.2007.09.032.

Wilkinson, K. D., T. Gan-Erdene, and N. Kolli. 2005. "Derivitization of the C-terminus of ubiquitin and ubiquitin-like proteins using intein chemistry: methods and uses." *Methods Enzymol* no. 399:37-51. doi: S0076-6879(05)99003-4 [pii] 10.1016/S0076-6879(05)99003-4.

Winn, M. D., C. C. Ballard, K. D. Cowtan, E. J. Dodson, P. Emsley, P. R. Evans, R. M. Keegan, E. B. Krissinel, A. G. Leslie, A. McCoy, S. J. McNicholas, G. N. Murshudov, N. S. Pannu, E. A. Potterton, H. R. Powell, R. J. Read, A. Vagin, and K. S. Wilson. 2011. "Overview of the CCP4 suite and current developments." *Acta Crystallogr D Biol Crystallogr* no. 67 (Pt 4):235-42. doi: 10.1107/S0907444910045749.

Wu, J., J. Li, F. Tian, S. Ren, M. Yu, J. Chen, Z. Lan, X. Zhang, D. Yoo, and J. Wang. 2009. "Genetic variation and pathogenicity of highly virulent porcine reproductive and respiratory syndrome virus emerging in China." *Archives of Virology* no. 154 (10):1589-97. doi: 10.1007/s00705-009-0478-6.

Yu, X., N. Chen, L. Wang, J. Wu, Z. Zhou, J. Ni, X. Li, X. Zhai, J. Shi, and K. Tian. 2012. "New genomic characteristics of highly pathogenic porcine reproductive and respiratory syndrome viruses do not lead to significant changes in

pathogenicity." *Vet Microbiol* no. 158 (3-4):291-9. doi: 10.1016/j.vetmic.2012.02.036.

Yuan, S., D. Mickelson, M. P. Murtaugh, and K. S. Faaberg. 2001. "Complete genome comparison of porcine reproductive and respiratory syndrome virus parental and attenuated strains." *Virus Res* no. 74 (1-2):99-110. doi: S0168170200002501 [pii].

Zeng, W., L. Sun, X. Jiang, X. Chen, F. Hou, A. Adhikari, M. Xu, and Z. J. Chen. 2010. "Reconstitution of the RIG-I pathway reveals a signaling role of unanchored polyubiquitin chains in innate immunity." *Cell* no. 141 (2):315-30. doi: 10.1016/j.cell.2010.03.029.

Zhao, C., M. N. Collins, T. Y. Hsiang, and R. M. Krug. 2013. "Interferon-induced ISG15 pathway: an ongoing virus-host battle." *Trends Microbiol* no. 21 (4):181-6. doi: 10.1016/j.tim.2013.01.005.

Ziebuhr, J., E. J. Snijder, and A. E. Gorbalenya. 2000. "Virus-encoded proteinases and proteolytic processing in the Nidovirales." *J Gen Virol* no. 81 (Pt 4):853-79.

Zikánová, M., J. Krijt, H. Hartmannová, and S. Kmoch. 2005. "Preparation of 5-amino-4-imidazole-N-succinocarboxamide ribotide, 5-amino-4-imidazole-N-succinocarboxamide riboside and succinyladenosine, compounds usable in diagnosis and research of adenylosuccinate lyase deficiency." *Journal of Inherited Metabolic Disease* no. 28 (4):493-499. doi: Doi 10.1007/S10545-005-0493-Z.

Zikánová, M., V. Skopova, A. Hnizda, J. Krijt, and S. Kmoch. 2010. "Biochemical and structural analysis of 14 mutant ADSL enzyme complexes and correlation to phenotypic heterogeneity of adenylosuccinate lyase deficiency." *Human Mutation* no. 31 (4):445-455. doi: Doi 10.1002/Humu.21212.

APPENDIX A

List of Author's Publications and Patents

Deaton, M. K., A. Spear, K. S. Faaberg, and S. D. Pegan. 2014. "The vOTU domain of highly-pathogenic porcine reproductive and respiratory syndrome virus displays a differential substrate preference." *Virology*.

Capodagli, G. C., **M. K. Deaton**, E. A. Baker, R. J. Lumpkin, and S. D. Pegan. 2013. "Diversity of Ubiquitin and ISG15 Specificity among Nairoviruses' Viral Ovarian Tumor Domain Proteases." *Journal of Virology* no. 87 (7):3815-3827.

Ray, S. P., **M. K. Deaton**, G. C. Capodagli, L. A. F. Calkins, L. Sawle, K. Ghosh, D. Patterson, and S. D. Pegan. 2012. "Structural and Biochemical Characterization of Human Adenylosuccinate Lyase (ADSL) and the R303C ADSL Deficiency-Associated Mutation." *Biochemistry* no. 51 (33):6701-6713. doi: 10.1021/bi300796y.

Connor, S. E., G. C. Capodagli, **M. K. Deaton**, and S. D. Pegan. 2011. "Structural and functional characterization of Mycobacterium tuberculosis triosephosphate isomerase." *Acta Crystallographica Section D* no. 67 (12):1017-1022.

Crimean-Congo hemorrhagic fever virus vaccine through simultaneous ablation its viral ovarian tumor domain protease's of deubiqutinating and deISGylating activities., Pegan SD, Nichol S, Bergeron E, **Deaton M**, University of Denver & Centers for Disease Control and Prevention, 91254-847593 (001500US)